UNIVERSITÀ
POLITECNICA
DELLE MARCHE

FACULTY OF ENGINEERING

Master's Degree in Biomedical Engineering

3D printable insole with TPMS lattice for relieving foot plantar pressure and shear forces

Supervisor:

Prof. Marco Mandolini

Co-supervisor:

Prof. Mazher Iqbal Mohammed

Degree thesis of:

Aya AlAjjan

Academic year 2021-2022

Acknowledgement:

This work has been achieved by the efforts of Universitá Politecnica delle Marche in Ancona, Italy, in collaboration with the University of Loughborough in England. All thanks and appreciations go to the department of Industrial Engineering and Mathematical Sciences at UNIVPM, as well as Prof. Mazher Mohammed, Prof. Richard Bibb and Dr. Petra Jones for their collaboration and contributions.

Abstract:

Human feet are subjected to pressure forces during walking or running. However, these pressures are not equally distributed over the entire regions of the foot. The increase of pressure in one area regardless of the others can lead to serious medical issues such as foot ulceration in diabetic patients. Plantar pressure and shear stress are the main components that contribute to this caution. Medical insoles are usually prescribed to prevent this critical situation or to treat the foot by decreasing the feeling of pain.

This study proposes a design of 3D printable medical insole that contains lattice structure of triply periodic minimal surfaces (TPMS) unit cells in order to relieve plantar pressure and shear stress on the foot. To test the eligibility of this topology, TPMS specimens were created using nTopology software and subjected to a finite element analysis. Samples from EVA foam and other lattice structures were also tested under compression and elasticity modulus was calculated. After comparisons, the most appropriate combination of cell size and strut diameter of TPMS unit cells was selected for both hard and soft sections of the insole. The resultant unit cells were utilized in the final design of a full insole with TPMS lattice structure, and another insole with Fluorite lattice structure.

Keywords: insole, lattice, TPMS, Gyroid, FDM, TPU

Contents

List of figures

List of tables

Chapter 1:

Introduction

Chapter introduction:

This chapter is the keynote to reading this thesis. It gives an overview of the proposed research, highlighting the scientific significance of it, and giving a quick brief of what the following chapters will be about.

1.1 Overview:

Some people have abnormalities or malfunctions in their lower extremities, which makes it hard for them to execute their walking function properly. Normally in this case, orthoses are prescribed upon visiting the doctor, but sometimes, foot inserts or medical insoles can be sufficient to relief the existing pain or to prevent escalating the malfunction to a serious disease. This kind of footwear is also needed in the case of having dermatological issues or, in critical cases, diabetes as they can prevent the formation of ulcers due to concentrated pressure on specific regions of the foot.

Medical foot insoles have proved to be extremely efficient in relieving foot pain while walking. They are available in the market of various properties and features. At the same time, they can be specifically designed for the patient by scanning their foot and modeling the entire insole based on that scan, in addition to recording the patient's pressure distribution over the foot and gaining a pedobarographic image. Prefabricated insoles are still very useful and easily obtained, but with the precision of custom-made insoles, higher levels of comfort can be easily achieved in spite of the effort and costs that can be elevated when customizing a medical insole for the patient.

Insoles exist as prefabricated, custom-made, with embedded pressure sensors, flat insoles, CAD-CAM insoles, manufactured with additive manufacturing techniques, containing lattice structure .. etc. In the end, no matter what the used method is, the ultimate goal of deigning a foot insole is to bring comfort to the patient, allowing them to perform their essential function wearing any kind of shoes they would like, and this is a tough goal to be engineered.

1.2 Purpose of the study:

Medical insoles exist in a plenty of shapes, sizes and properties. They can be manufactured using various methods and techniques, of which is additive manufacturing, the extremely advanced method with the aid of computer software. Additive manufacturing made it easier to build any object by layering it according to the user's preferences and application requirements. As an additional perk, since insoles are an extra part to be added to the shoe, the patient will definitely prefer it to be extremely comfortable and more importantly, very lightweight. This also impacts on the financial value of the product.

Therefore, based on the definition of lattice structure which enlarges the volume using less material, a new design of a medical insole containing lattice structure was proposed. R. Simone [5] has initiated the research in 2021 using graphic unit cells and put some future goals in the end of it. Hence, this study comes along as a continuation and achievement of the future goals, alongside trying more concepts in the same field.

In conclusion, this study tested Octet, Fluorite, Face Center Cubic, Gyroid and Schwarz P unit cells under compression, in addition to EVA foam that is usually used in prefabricated insoles. After analyzing the data, the best unit cells were Fluorite and Gyroid with certain values of cell size and strut diameter. Two insoles with lattice structure of the aforementioned unit cells were designed and meshed for 3D printing at a later time.

1.3 Content preview:

This study is explicitly explained in the pages of this thesis. It consists of six chapters. Each chapter discusses one aspect of the study as the following:

- ***Chapter 1: Introduction***

  This chapter presents a brief introduction to the medical problem that is addressed in the study, listing the available solutions and suggesting new

ones. Then it briefly talks about the purpose of this study. Finally, it provides an overview of the other chapters of the thesis.

- ***Chapter 2: Literature Review***

  This chapter lists some of the reviewed approaches from the scientific history which serve the same purpose of the suggested study, i.e., modeling custom-made insoles via different methods. Each reviewed study is explained in terms of aim, methodology, results and conclusion.

- ***Chapter 3: Scientific Background***

  Any problem that is in need of a solution, requires basic knowledge prior to starting with designing the solution. For that reason, this chapter explains the basic scientific concepts (the pressure forces that impact on the foot and everything about medical insoles) that will help the engineer know what to choose in their design process.

- ***Chapter 4: Methodology***

  After looking at the theoretical background of the problem and solution, practical information must be collected. This chapter explains the engineering fundamentals which were used in the design process, hence lattice structure definition and material properties.

- ***Chapter 5: Case Study***

  This chapter elaborates on the real execution of all the gathered information and data, starting from virtually simulating lattice structures under pressure force to experimentally subjecting the structures to real force pressure. The final outcome of this chapter is a full insole with TPMS lattice structure.

- ***Chapter 6: Results & Discussion***

  This chapter finalizes everything in this study, explaining and discussing every detail in the results of simulation and design. It also includes the overall conclusion and future goals of the research.

- ***References***

  These pages list the citations that were referenced in this study.

Chapter 2:

Literature Review

Chapter introduction:

Science and technologies are in a constant advance, especially when it comes to biomedical engineering; the science that has to be always up-to-date with all the approaches that are being or will be made in the favor of medical healthcare. Therefore, to start new research, an engineer must look through previous approaches to get inspired or even come with a new concept that can enrich the scientific content of the same interest. This chapter reviews some of the previous papers that were published about designing custom-made insoles for 3D printing using different additive manufacturing techniques or any other methods.

2.1 Adjustable modulus porous structures for insoles:

In 2018, Z Ma et al. [1] presented a study on the porous structural units regarding the geometrical parameters, porosity, and their relationship with the effective modulus. In this paper, the mathematical relationships between the effective modulus and the basic geometrical parameters were derived and subsequently used to construct an insole model.

Material extrusion technique (MEX) was used by the researchers here because in their opinion, among all kinds of 3D printing techniques, MEX is a commonly used technique due to its low cost in equipment and materials, which makes it a fairly good option for fabrication. Regarding the material to be used, they reported that common flexible materials, like thermoplastic polyurethane (TPU) and thermoplastic elastomer (TPE), have effective moduli that are beyond the demand of alleviating plantar pressure.

At first, porous structural units were designed by parametric modeling. Among all units, the ellipsoidal structural unit (as shown in Figure 2.1) was employed in this study because of its relatively satisfying 3Dprinting quality and resilience under compression. [1]

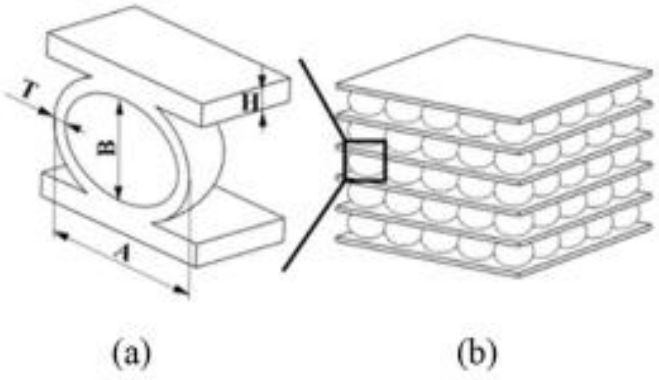

Figure 2.1: (a) ellipsoidal unit cell of the porous structure. (b) sketch of arrayed samples [1]

During compression, samples were compressed at a constant speed of 1 mm/min, with a sampling frequency of 120 Hz. Tests were suspended when the force reached the upper limitation of 200 N, in order to keep the samples within linear elastic range and avoid plastic deformation or internal structure interference. Compression testing simulations of various porous structure models were carried out via FEA method in ABAQUS.

Overall, the effective moduli determined from the FEA simulation vary from 0.27 MPa to 3.68 MPa, which are 40.5% ± 10.3% lower than those derived from compressive tests. In conclusion to their results, they reported that the elliptical unit possesses flexibility in adjusting its geometric size as well as its effective modulus, which enables this porous structural unit to satisfy both geometric and mechanical demands of designing the diabetic insoles or other possible applications. It could maintain its linear elasticity under normal plantar stress conditions, as shown in the stress-strain curves of sequential models in Figure 2.2. The yield strength of ellipsoidal unit is far beyond the maximum pressure which merely equals several times of normal plantar stress. With the increase of load, the internal structures pile up and the effective modulus increases, like the latter range of stress-strain curves. [1]

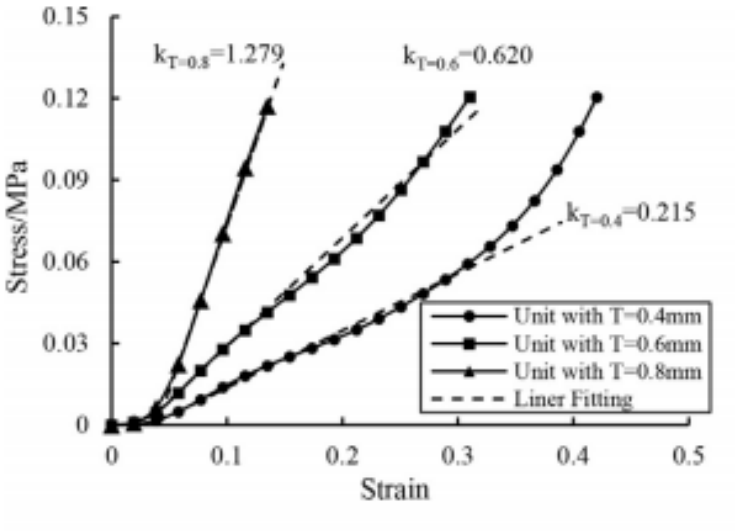

Figure 2.2: Stress-strain curves of the sequential models [1]

2.2 Customized 3D printed foot orthosis:

In 2014, O. Ciobanu et al. [2] designed a 3D printable customized insole based on 3D scanning of the foot. The purpose of this design was to achieve an improvement in gait comfort and effort, as well as foot-loading characteristics and a reduction in fabrication time and cost compared to conventional customized foot insole fabrication techniques.

They used the basic stages of Rapid Prototyping that consist of 3D scanning the foot, reconstruct the 3D surface, build the CAD model then converting it to an STL format to be available for printing. The material that was used in this project was Acrylonitrile butadiene styrene (ABS). Their final result of this process was as shown in Figure 2.3. [2]

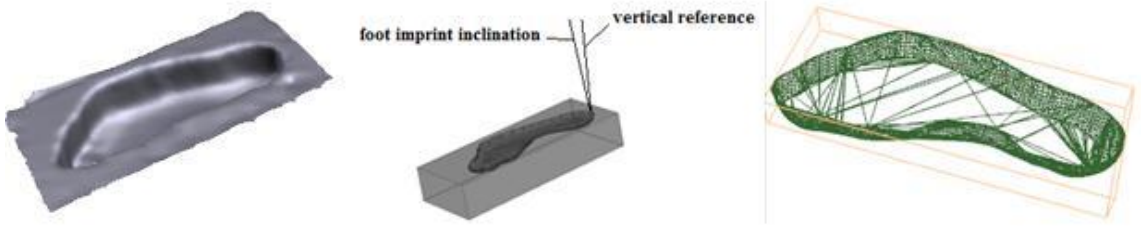

Figure 2.3 Foot imprint, inclination, cutting foot insole shape, respectively [2]

2.3 Development of 3D printed insoles:

The main objective of the study was to print a pair of customized insoles based on foot scanning. In 2020, S. Jandova et al. [3] developed a custom-made 3D printable insole using PolyJet Matrix technique of 3D printing. In their opinion, patient comfort is a complicated issue in the design of footwear. The proper fit may be dictated by several factors such as shape, size, weight, materials among others and it is also necessary to take into consideration measurements such as heel width, heel to ball width, heel to ball length, toe box space among others.

For that purpose, they ran an experiment where the participants were asked to perform 10 steps (5 left and 5 right). These steps were later analyzed, from which the average values of the foot length, forefoot width, heel width, plantar angles and Arch index were observed. Recording the plantar pressure occurred when walking barefoot and when wearing the insole separately. Wearing the insole showed a positive effect in terms of balance and posture stabilization during stance phase. [3]

2.4 Customized footwear with improved comfort:

The most recent paper that was published was in 2021, by R. Teixeira et al. [4]. This research aimed to design 3D printed graded density inserts to be placed in one of the critical plantar pressure regions of conventional insoles; the heel. Using slippers made of TPU, these inserts were mechanically tested and their comfort was qualitatively assessed by a group of subjects. Their basic concept was that there are some factors that can be related to the perceived shoe comfort, such as interior softness, thermal comfort (temperature and humidity), flexibility, weight, damping capability, heel zone impact absorption, and plantar pressure distribution, among others.

Fused Filament Fabrication (FFF) seems to be the most adequate technique to solve this problem, mainly due to the geometrical freedom it provides, when compared to the conventional manufacturing processes, and to the vast range of materials that it can use. In addition to the geometrical freedom, it also enables the combination of several different materials in the same component, when multi-

material FFF techniques are adopted. In this case, flexible and rigid materials, opaque and transparent materials, or different colors of the same material, are just a few examples of the combinations that can co-exist in a single printed part. The used material was Filaflex, a polyurethane based thermoplastic filament, with Shore A 82.

The main stages of their work were characterizing uniform mesh density structures, generating graded density structure inserts, and producing and assessment of prototype slippers. Graded structure was designed by selecting the triangular mesh and different filling densities for the internal structure of the samples. The triangular geometry was selected since it facilitates the automatic generation of graded density meshes. Several filling densities were tested (0, 10, 15, 20, 25, 40, 50 and 100%). densities. When the filling density varies from 10 % to 50%, the resulting cell size varies from around 11 mm to 2 mm. Figure 2.4 shows the different samples that were later tested in the compression test for analyzing stress-strain curves. [4]

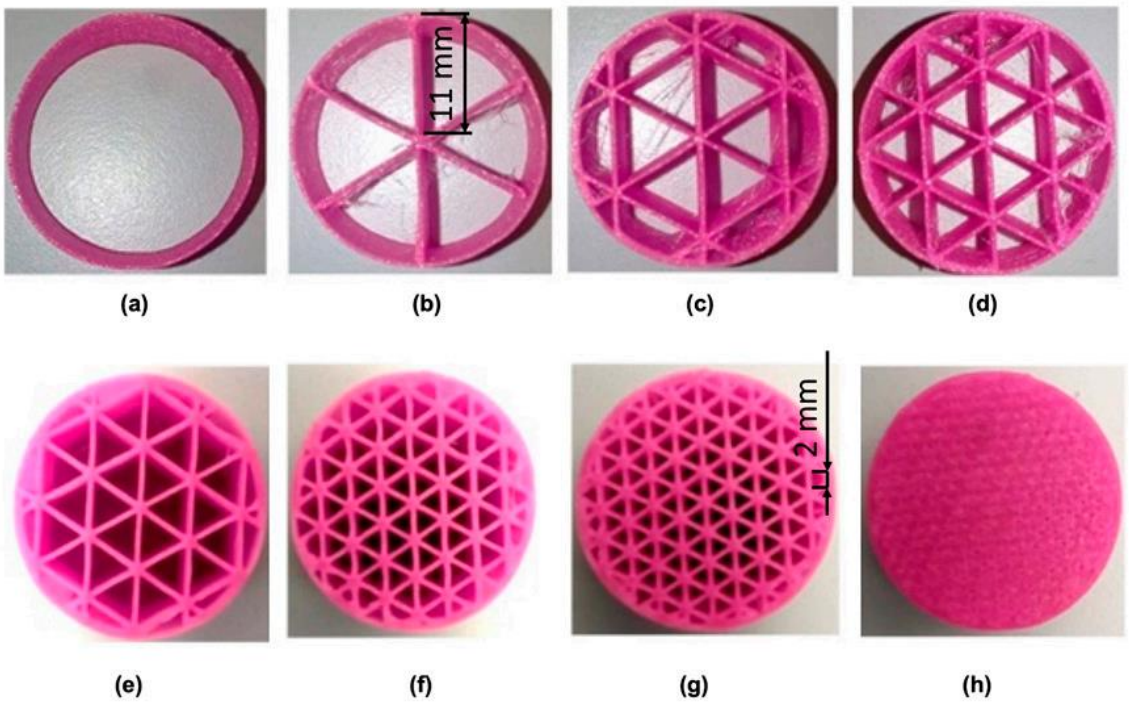

Figure 2.4 Printed samples, for compression tests, with different filling densities (triangular mesh): (a) 0%; (b) 10%; (c) 15%; (d) 20%; (e) 25%; (f) 40%; (g) 50%; (h) 100% (dimensions in mm) [4]

As expected, increasing filling densities results in higher structure stiffness (higher modulus and maximum stress), i.e., with the same material, different meta-properties for the structure are obtained, which may vary within a wide range. Three different

regions of the stress-strain curves were identified: 1) linear region of the stress-strain curve, where the stress increases proportionally to the strain imposed to the material, 2) region where the structure deformation takes place, due to the buckling of the vertical walls, where the strain increases at almost constant stress (the stress at yielding) and 3) densification region where the stress starts again to increase, due to the full collapse or crushing of the structure. Figure 2.5 shows the stress-strain curves of the tested samples.

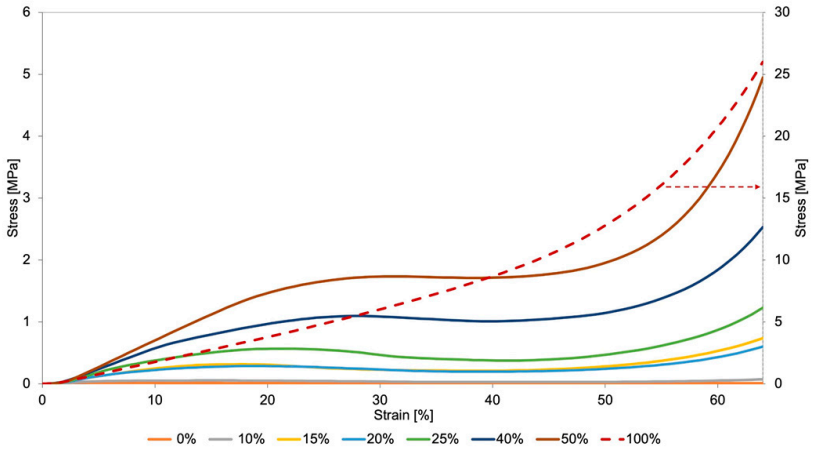

Figure 2.5 Stress-strain curves of different densities of the material [4]

The results obtained in the compression tests of the uniform mesh density structures revealed optimum values corresponding to 10% to 50% filling densities, i.e., a range adequate for insole applications. After determining the effect of using different filling densities, the next step consisted in the generation of inserts with graded mesh density structures adjusted to the plantar pressure distribution. The prototype slippers and the reference ones were tested by a group of participants and in conclusion, the prototype slippers performed better than the reference ones in what concerns to the maximum deceleration. [4]

2.5 Design of 3D printed custom-made orthopedic insoles:

In 2021, R. Simone [5] carried out his graduation thesis at Università Politecnica delle Marche and it is the base core upon which this research is built. It aimed to design a custom-made insole that contains lattice structure, testing different graphic unit cells, to relieve the plantar pressure and shear force in the diabetic foot.

To define the best structure that suits the application of a comfortable custom-made insole, samples were designed in nTopology with different unit cell types, sizes and strut diameter. They were printed using TPU powder in SLS technique. After virtual simulation, the best unit cells were defined thus used in designing the full insole by two methods; maintaining the cell size and grading the strut diameter according to a pressure map of the foot, and maintaining the strut diameter while grading the cell size according to the same pressure map where it warps the cell map of the lattice. Figure 2.6 shows the final design of the insole in the aforementioned methods. [5]

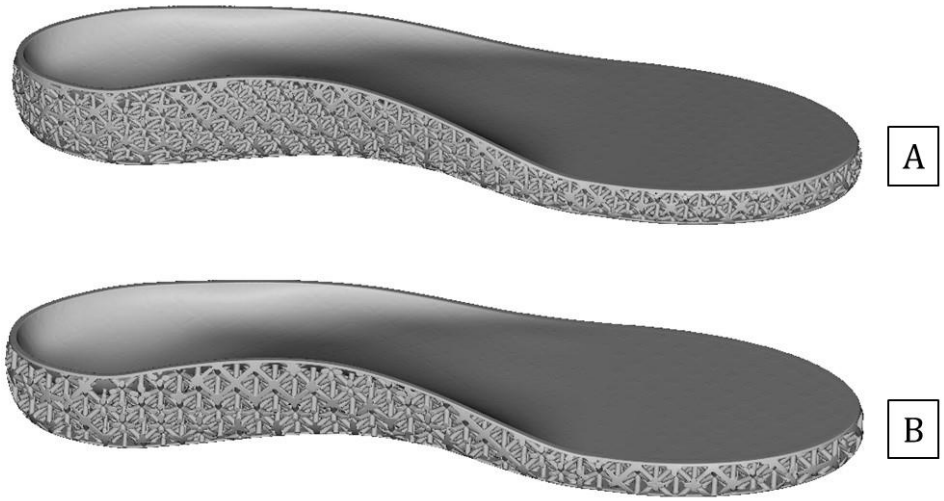

Figure 2.6 Final insole design. A) Grading cell size. B) Grading strut diameter [5]

The future goals of this study were to run compressive tests on the printed samples in order to assess the real performance of the lattice structure, as well as looking for other lattice structures to be used in this application. These goals are to be addressed in the current thesis.

Chapter 3:

Scientific Background

Chapter introduction:

In order to define the essential properties when designing an insole, one should know everything that concerns the foot anatomically, the geometry, the material science and mechanical aspects of the design. This chapter highlights the basic concepts that are required to start an insole design.

3.1 Forces that impact on the foot:

Pressure force on the foot is a very important factor that can lead to better evaluation of gait effectiveness, as well as the discovery of abnormalities in walking cycle. Detailed studying of the pressure can also be useful in preventing future ulceration, especially with diabetes patients. However, it is not unified in the whole area of the foot nor in the entire population; foot pressure is distributed differently from one person to another. This distribution depends on various factors such as age, walking speed, stride length, step force and more. These things may change due to anatomical and physical reasons over time.

There have been plenty of studies that demonstrate the foot pressure distribution and its changing factors. One of these studies is an experiment that was carried out by Jo Hessert et al. [6] where they measured force pressure distribution (FPD) with 9 young (30 ± 5.2 years), and 6 elderly subjects (68.7 ± 4.8 years) during normal walking speed using shoe insoles with 99 capacitive sensors. Figure 3.1 shows the distribution of foot pressure over the different regions of the foot from their experiment. As the figure shows, the highest values of pressure and loading are located in the medial calcaneus and medial hallux. The end result of their study showed that the elderly people tend to bear their weight on their lateral side rather than the medial side as in young people. Therefore, they have lower values of normalized maximum pressure and mean pressure in the medial calcaneus and hallux area, as an example of the difference in distribution due to age.

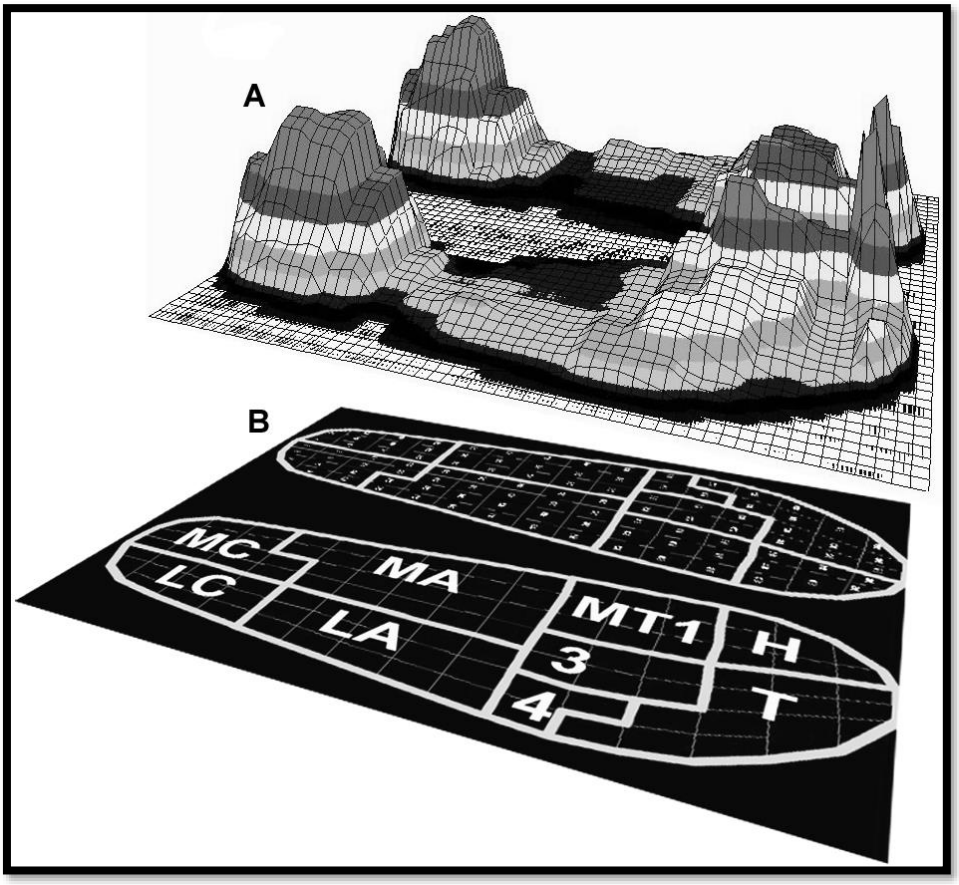

Figure 3.1 A) Distribution of foot pressure during stance phase. B) Anatomical mask superimposed on the insole ((MC = medial calcaneus, LC = lateral calcaneus, MA = medial arch, LA = lateral arch, MT1 = first metatarse, 3 = second and third metatarse, 4 = fourth and fifth metatarse, H = hallux, and T = toes) [6]

Another study by Hayafune et al. [7] carried out an experiment to determine the pressure distribution regions in the foot during push-off phase using a standard mesh configuration. Their method involved 42 healthy subjects (23 women and 19 men) aging from 20 to 59 years. They found the highest pressure to be found in the big toe region and the region under the second metatarsal head. Figure 3.2 shows the foot pressure distribution over 10 anatomical areas after subdivision and it clearly demonstrates that the highest peaks of pressure occur at the medial toe, medial metatarsal and medial calcaneus, which corresponds to the aforementioned study.

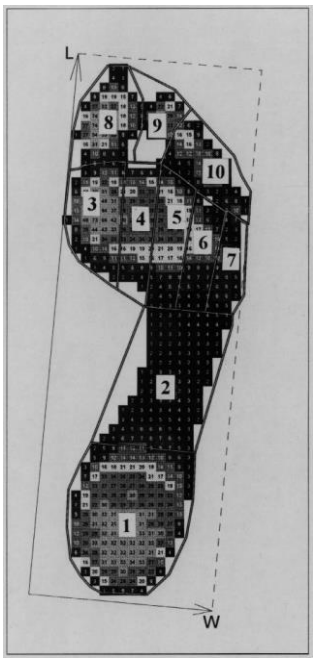

Figure 3.2 The automatically generated Novel grid as used to subdivide the sole of the foot [7]

With deeper investigation, research focused on two significant values that have a major impact on gait effectiveness and lower limb pathology; plantar pressure and shear force.

3.1.1 Plantar pressure:

Plantar pressure is defined as the pressure between the plantar surface of the foot (sole) and the supporting surface. When it comes to dangerous threats, plantar pressure becomes a critical factor that can lead to ulceration, especially in diabetes patients. Accumulated stress over the area of the foot where the pressure is high causes neuropathic plantar ulcerations, alongside joint impairments or deformities. Plantar pressure can be measured using various methods; among them is a set of sensors inside the insole or between the shoe and the plantar surface of the foot. By measuring plantar pressure, assessment of the foot pathologies or abnormalities can be achieved [8]. Plantar pressure plays a major role in identifying foot pathologies that are related especially to human locomotion. Figure 3.3 shows the ideal plantar pressure distribution over the contact area of the foot during various gait phases [9]. High or abnormal values of plantar pressure can cause asymmetry in the pressure distribution between the two feet, which disturbs a perfect gait cycle. If this

asymmetry can be quantified, identification of foot pathologies and gait abnormalities can be achieved, thus orthotic solutions can be found for that specific problem [9].

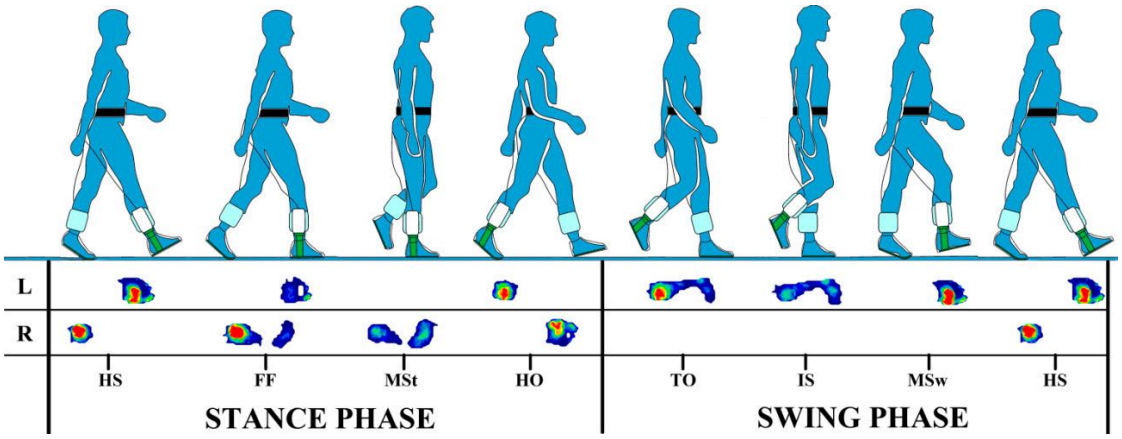

Figure 3.3 An example of in-shoe plantar pressure measurement during gait phases [9]

Wafai et al. [9] have studied the effect of plantar pressure asymmetry on the gait cycle and how it can help identify pathologies. According to them, higher values of pressure may lead to several disturbing situations where they may inflict further high pressure onto a new area of the foot or increase the risk of imbalance for the walking person. In addition, it will increase the chance for asymmetry of plantar pressure distribution between the two feet to happen. To understand that practically, they gathered 51 participants (31 individuals in control group and 20 individuals in pathological group) to collect data. The pathological group had misalignment in the lower limb, which caused them to suffer from painful regions on the contact area of the foot. They used a mask to subdivide the pedobarographic image into 10 anatomical areas as shown in Figure 3.4. These locations correspond to (1) interphalangeal joint (IPJ); (2) lesser toes; (3) metatarsophalangeal joint 1 (MPJ1); (4) MPJ2; (5) MPJ3; (6) MPJ4; (7) MPJ5; (8) midfoot; (9) medial heel; and (10) lateral heel. The output of plantar pressure measurement gave visual feedback to assist in defining the malfunctioned areas of the foot. An example of the asymmetry of plantar pressure distribution between the two feet in pathological group, specifically in metatarsalgia, is shown in Figure 3.5, where the colored legend represents pressure values from low (dark blue) to high (red).

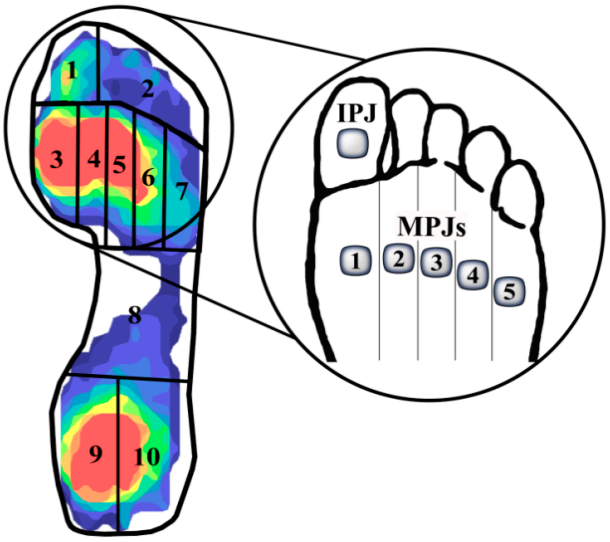

Figure 3.4 Mask of 10 anatomical regions of interest [9]

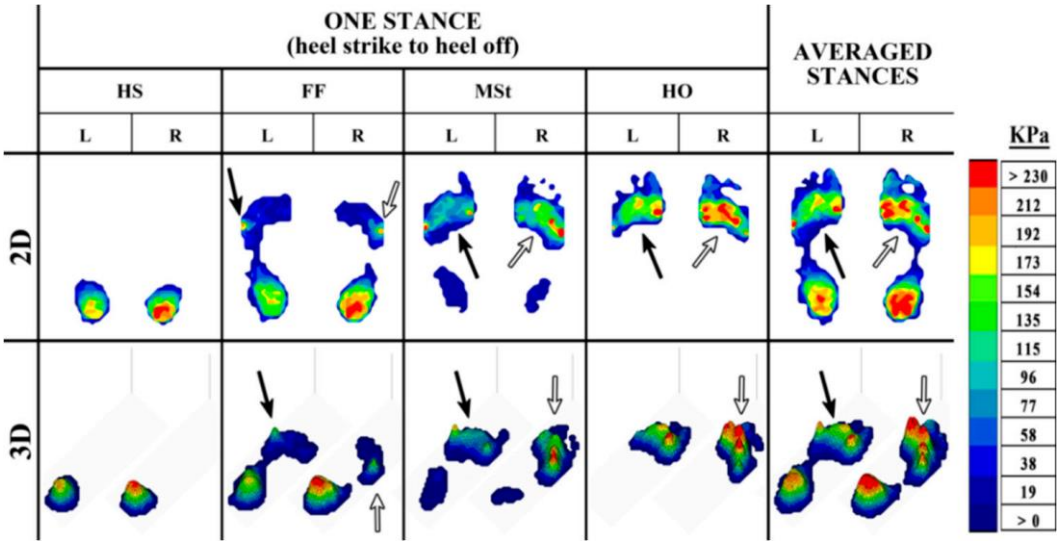

Figure 3.5 Plantar pressure distribution in metatarsalgia in the pathological foot during stance phase [9]

Asymmetry levels between the two feet were determined from the normalized peak plantar pressure parameters at 10 anatomical regions of interest for the control and pathological groups. In this way, the variation of peak pressure between the two feet helped identify the level of asymmetric distribution, which emphasizes the fact that plantar pressure is really helpful in determining foot pathologies [9].

3.1.2 Shear stress:

Another important force is shear stress, which is the yielded force of anterior-posterior axis and mediolateral axis upon presuming a sensor shift as depicted in Figure 3.6 [10].

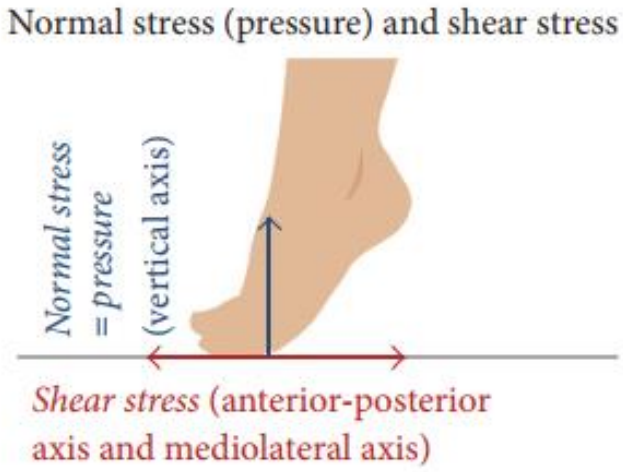

Figure 3.6 Normal stress (pressure) is vertical axis. Shear stress in on the horizontal axis [10]

According to Amemiya et al., shear stress is a major contributor to having severe diabetic foot ulcer, especially when it is associated with callus. This even led to the need of having a valuable ratio that is equal to the shear stress over the normal stress (SPR). This ratio ranged from low to high, indicating an area of callus formation, which helps defining the severity of the diabetic foot ulceration, therefore choosing the best footwear to heal [10].

Also, in a systematic review carried out by D. Jones et al. [11], researchers aimed to review papers about the significance of shear stress in the case of diabetic ulcers as it forms a major part of plantar load. They searched through Ovid Medline, EMBASE, CINAHL and Cochrane library databases in order to collect 1461 articles, among which 16 studies met their criteria. They basically chose studies that involved participants' groups that had previously/currently diabetic ulcers plus healthy groups. This was to determine whether diabetic ulceration is caused by higher shear stress or not.

The studies that compared shear stress in patients with current/previous diabetic ulcers and patients without diabetic ulcers had proven that shear stress with diabetic ulcers is much higher than without it. Other studies that compared shear stress in diabetic patients and healthy individuals had also proven that shear stress is higher in the presence of diabetes. Regarding callus formation, some studies have found no difference in shear or peak pressure between individuals who had callus and others who did not have callus [11].

In conclusion, plantar pressure as well as shear stress distribution are important factors to help define human locomotion problems and lower limb abnormalities. When there is a noticeable malfunction, orthotic footwear and insoles may be essential.

3.2 Medical insoles:

Just like any other treatment manner, medical insoles are required to treat or prevent the occurrence of foot pathologies. Louisville Orthopaedic Clinic [33] provided an interesting guide, introducing insoles and their essential value in human locomotion treatment.

What are the insoles?

Foot orthotics are in-shoe devices that are used to treat or prevent an injury, pain or disability. They come in two categories; prefabricated (over-the-shelf/counter) which are less expensive, easily made and generally shaped, and custom-made which take longer time to design and manufacture and are more expensive but definitely more effective and patient-appropriate [12]. They are sometimes called arch support because they get put inside the shoe to support the foot arch basically. They vary from rigid plastic material to shock absorbing material to containing layers of both types of material. They come in different sizes and shapes to accommodate the patient and their special condition. Some of them support the midfoot like the metatarsal pad which is used for patients with pain in the ball of the foot. Other types are heel supporters or heel cushions that are inserted into the insole [33].

When does an individual need an insole?

According to Louisville Orthopaedic Clinic, problems in the alignment of the ankle and the foot might not only cause ankle and foot issues but also hip, knee and even back issues. In that case, the doctor prescribes a special orthosis or insole to solve some biomechanical issues with the patient such as flat foot in diabetes or overpronation [33].

Why does an individual need a custom-made insole?

Prefabricated insoles can be useful to treat minor injuries or mild biomechanical abnormalities, while custom made insoles will be designed appropriately to accommodate with the patient and their own case. An imprint of their foot is taken and considered as the basic reference upon which the insole is designed. This can also be an advantage as the patient can wear the insole with any type of shoes since it will be custom-made for all required cases [33].

How are insoles made?

Orthotics are fabricated using several technologies. In the past, a type of casting or molding was the standard method to make a custom-made insole. This means that a therapist or orthotist uses plaster gypsum strips to create a mold of the foot. The orthotic is made by filling in the mold and correcting any abnormalities if necessary. Another popular method is the foam box. The patient steps into a box of foam-like substance, similar to a memory foam mattress or pillow, and leaves an impression of the feet. More recently 3D computer images have been implemented to assess abnormalities and guide the manufacturing of a custom-made orthotics [33].

This raises an interesting question; are custom-made insoles worth the effort and the cost that relate to them? How do they perform comparing to the traditional prefabricated insoles?

3.2.1 Custom-made vs. prefabricated insoles:

In 2010, the Canadian Agency for Drugs and Technologies in Health issued a report [12] involving a review of systematic reviews about the clinical and cost-

effectiveness of prefabricated and custom-made insoles. After searching several resources like PubMed, CINAHL, The Cochrane Library, University of York Center for Reviews and Dissemination (CRD), ECRI (Health Devices Gold), EuroScan and international health technology agencies, they identified four systematic reviews that included orthotic devices. These four are:

1. A Cochrane review in 2008 that assessed custom-made orthotics that are used for **treating foot pain** in comparison with prefabricated orthotics and sham insoles. Patients in this review had juvenile idiopathic arthritis (1 study), rheumatoid arthritis (1 study) or plantar fasciitis (3 studies). However, none of those studies showed a statistically significant difference between groups with the two categories of insoles, regarding the change in foot pain or improvement in function after 6 weeks to 12 months of follow-up.
2. The second review evaluated several interventions for **treating plantar heel pain and fasciitis**. It involved comparing custom-made insoles with prefabricated orthotics and placebo shoe inserts. In conclusion, both categories were equally effective in decreasing plantar heel pain.
3. A systematic review by Aaltonen et al. in 2007 that assessed interventions used to **prevent sports injuries**. It included 32 studies, among which five studies compared the injury rate between military recruits using custom-made, prefabricated insoles or using no insoles at all. There was no difference between the groups regarding the event of lower extremity injuries. Therefore, custom-made and prefabricated insoles were equally effective in avoiding lower limb injury in military recruits.
4. The fourth review assessed foot orthotics to **prevent or treat overuse conditions of the lower extremity**. It concluded that there was no difference between custom-made and prefabricated orthotics for the prevention or treatment of overuse conditions of the lower extremity [12].

In another study in 2020, D'Amico et al. [13] aimed to compare the pressure-relieving efficiency of traditional shape-based total contact customized insoles (as

they referred to it by TCCI) with sophisticated CAD-CAM approach. Involving 30 neuropathic diabetic patients, they ran an experiment to evaluate the risk regions of interest and their areas during stance phase in three different walking conditions: flat insole (FI), TCCI and CAD-CAM insoles. Flat insoles were made of 12.7-mm-thick ethylene-vinyl acetate foam (EVA with shore 40) and they were provided within wearable sandals. Foam impression of the feet was taken then 3D scanned to fabricate total contact custom insoles (TCCI). They were fabricated using individual positive plaster molds.

The final result of their experiment was that compared with FI, both TCCI and CAD-CAM insoles provided a decrease in the risk regions, especially that CAD-CAM performed even better than TCCI. This means that custom-made insoles provide less risk and reduce peak pressure in diabetes patients, better than just flat or prefabricated insoles [13].

In 2019, R. Xu et al. [14] carried out an experiment to compare the effectiveness of custom-made insoles against prefabricated insoles, where 80 patients with bilateral flatfoot participated. The subjects were divided in 2 groups; experimental group wearing 3D printed EVA customized insoles, and control group wearing prefabricated insole. The Footscan® system recorded peak pressure, peak force, and peak contact area in 10 areas of the sole at weeks 0 and at week 8.

- In the **mid-foot** area, compared with the control group, the peak pressure in the experimental group was significantly higher at week 0 and week 8, showing that the customized insole had better effect on appending the foot load and improving the joint deformity in patients with symptomatic flatfoot, and the customized insole was better than the prefabricated insole.
- In the **heel** area, the results indicated that the customized insoles did not differ significantly from the prefabricated insoles in terms of pressure, force, and contact area.
- In the **metatarsal** area, compared with the control group, the peak pressure of the 3rd metatarsal area in the experimental group was lower than that of week 0. This might indicate that the customized insole can more

effectively reduce the load on the plantar metatarsal region in comparison to the prefabricated insole.

- In the **toe** area, there was no significant difference between the 2 insoles.

In conclusion to that study, customized insoles had a better comfort level than prefabricated insoles. They reduced the load of the metatarsals and distributed the load to the mid-foot area to reduce lesions of the foot in patients with symptomatic flatfoot [14].

3.2.2 Insole designing properties:

When designing a customized insole, several properties need to be satisfied as much as possible. Compromises sometimes need to be made in the favor of achieving the best result that can guarantee high comfort for the patient. According to Cavanagh PR et al. [15], insoles with a vivid thickness have shown to be dramatically associated with lower values of pressure, while there was no noticeable relation between the stiffness and peak pressure as Birke JA et al. reported [16]. However, Stephen FA et al. [17] demonstrated that rigid insoles have shown to be useful for reducing regions of increased plantar pressure and enlarging the contact area. Moreover, more flexible insoles have proven to reduce plantar pressure than the less flexible ones. They should be designed as if they have a good foot arch restoring area, as well as a well-supported area for the ankle. Figure 3.7 shows an example of good relieving insole shape [7].

Figure 3.7 Low-flat unsupported arch and ankle (right). Restored foot arch and properly supported ankle (left) [7]

Another important property when designing insole is to compromise between thickness and hardness. As it turns out, the hardness of the insole may have an effect on its capability of reducing plantar pressure in different areas of the foot. Yao Meng et al. [18] carried out an experiment to test the effectiveness of various ranges of hardness of custom-made insoles on plantar pressure redistribution during walking and running. Their experiment involved six male subjects who were healthy and had no deformities in their lower limbs. The insoles that were used in the trial were of three types: flat control insoles that were prefabricated of foam with Shore C of hardness 30, custom-made hard insoles (CHI) with hardness of Shore A150 and custom-made soft insoles (CSI) with hardness of Shore A75. Both custom-made insoles were made of two layers; the upper is from foam and the lower is from thermoplastic material as shown in Figure 3.8. Participants were asked to walk and run with normal speed wearing these three types of insoles. Plantar pressure was then measured and peak pressure, mean pressure, maximum force, pressure-time integral were analyzed.

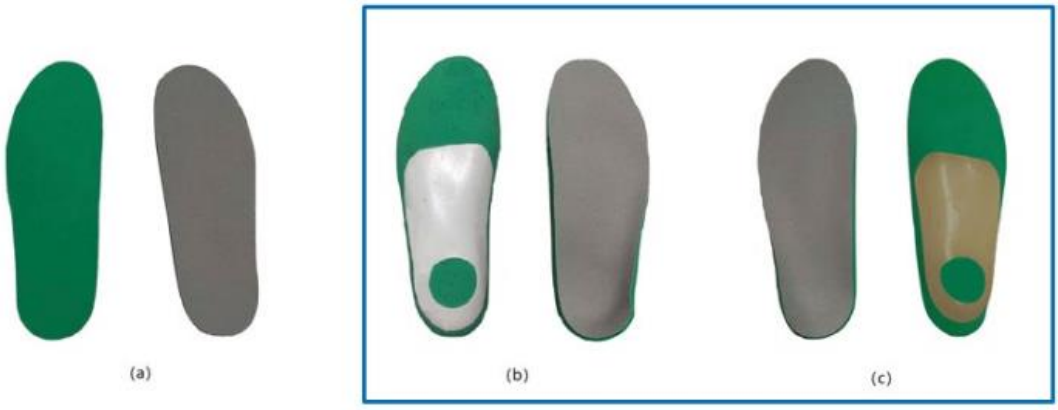

Figure 3.8 a) control insole, b) custom insole with soft material, c) custom insole with hard material [18]

The results of this study showed that plantar pressure of forefoot and medial midfoot were enormously increased wearing both custom-made insoles, as well as the plantar pressure of the lateral forefoot and lateral midfoot. On the other hand, hard insoles increased the plantar pressure of the medial forefoot a lot more than the soft or control insoles. Therefore, after analyzing the data, they found that custom-made insoles can appropriately support the foot to redistribute the plantar

pressure over the entire area and alter the pressure of other regions and arch. They also suggested that custom-made soft insoles seem better than custom-made hard insoles because hard insoles lead to highly increased pressure at medial forefoot, which can cause pain in the forefoot [18].

3.2.3 Effect of materials on insole fabrication:

In a systematic review of the effect of different orthotics material on plantar pressure, M. Gerrard et al. [19] have reached a result of collecting data about the best materials to be chosen for designing an insole or a footwear piece. After searching through multiple resources such as MEDLINE, CINAHL, Embase and SportDiscus, as well as hand searching, they ran a statistical analysis to choose the most criteria-fulfilling among all. The final result was sorting five studies that had a Quality Index score between 20 and 23.

Those studies investigated different materials like polyurethane [20,23,24], polyethylene [23,24], ethyl vinyl acetate (EVA) [20,21] and carbon graphite [22]. Besides investigating these materials, they used different masks for anatomically dividing the foot based on plantar pressure distribution. Polyurethane -as in open cell foam- was found to decrease peak pressure all over the foot areas in low and medium densities. EVA was tested in two of the studied and in two density classifications too; low and medium. Low-density EVA reduces peak pressure slightly at the first metatarsal and hugely at the lateral metatarsals. Carbon graphite has the least effect of all; it decreases the contact area under the foot, almost slightly to mediumly in all the anatomical sections.

The most important note extracted from this review is that polyurethane and polyethylene were found to lead to massive changes in plantar pressures. Polyurethane is the most desirable as it reduces peak pressure across all anatomical sections of the foot. Moreover, 3 mm polyurethane reduces peak pressure better than 3 mm EVA. To use the optimum properties of it, plantar forces should be distributed over a larger area by enlarging plantar contact area [19].

In another study made by E. Hermansson and E. Marcus [25] in 2019, the aim was to evaluate if additive manufacturing (AM) is an appropriate manufacturing method for insoles in comparison to vacuum forming (VF) and subtractive manufacturing (SM) in regards of material properties. They reported that materials that have a low coefficient of friction will help decrease the shear stress of the insole. Depending on the density and thickness, the material will either have better stability properties or shock absorption properties. If the material is too thin or soft it will easily scar and tear.

In their opinion, the mechanics to be considered are: shock absorption, friction, Hooke's law (when a stress/strain proportionality can be identified, the modulus of elasticity is this proportionality when the properties of the material are elastic), shear stress and material fatigue. One participant was the subject of their experiment, testing 3 types of insoles: VF and SM insole made of EVA foam sheet, and AM insole printed with FDM and made of TPE [25].

A pattern of rectangular cuboids was created inside the samples, this would theoretically increase the shock absorption. It was noticed that the mean weight of the AM sample (made with TPE) was a lot higher than those of the VF samples (made with EVA). When calculating the mean density of the AM sample, it was also noticed that AM had a higher mean density than the VF samples.

In conclusion, to decide the internal structure of a closed cell design, the desired shock absorption, mass, impact strength, cell pattern and the limitations of the printer must be known [25].

Chapter 4:

Methodology

Chapter introduction:

After knowing the medical requirements and previous approaches to the design of a comfortable insole, basics should be listed to be chosen and used in the real work. This chapter elaborates on the practical methods of lattice structure, unit cell type, material and software to be further used in the case study.

4.1 Lattice structure:

Lattices are an excellent way of generating light-weight, yet highly strong, parts that can also significantly reduce the time and cost it takes to make AM parts. Lattice structures offer a major advantage in reducing part weight without greatly affecting part strength, which is very important in industries such as aerospace and transportation [26]. They are cellular structures that refer to a wider classification of naturally occurring and engineered structures that tesselate to fill space as shown in Figure 4.1. These cellular structures may either be closed cell, for example, as first observed in the structure of cork by Robert Hooke, or open cell, for example in naturally occurring honeycomb structures [27].

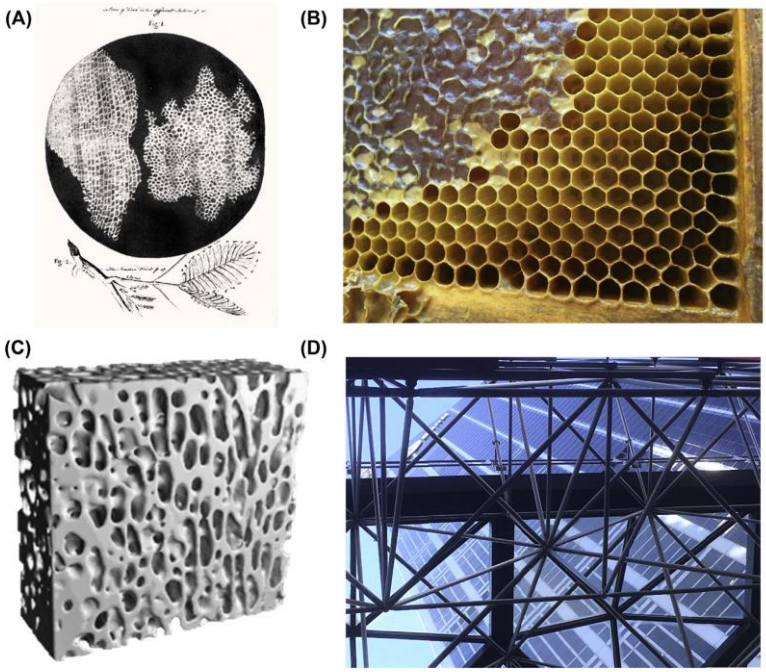

Figure 4.1 Cellular and lattice structures: A) First observation of lattice for cork, B) open hexagonal structure in honeycomb, C) naturally occurring lattice in trabecular bone, D) Civil engineering lattice [27]

A lattice is a cellular structure made of repeated unit cells to form a larger volume [26], or in other words, they refer to the open-celled arrangement of strut elements with defined connectivity at specified nodes [27]. Lattice structures are often observed in both naturally occurring biological systems such as the cellular structures of trabecular bone, and in engineered structural systems. Lattice structures may have either stochastic or periodic arrangements. Biological lattice systems generally feature stochastic arrangements, whereas engineered lattice structures are typically periodic [27].

There are many options for the shape and size of such lattice cells, and for the pattern in which they are repeated, and there are countless examples of lattice structures being used to reduce the amount of material used in a part to improve its strength to-weight ratio, or to replace support material in a part. Lattices can be uniform, where the same cell size is repeated in all directions of the part, or variable, where the size and spacing of the cells is different in different directions. Variable lattice structures are popular in medical applications, such as implants, because the variability of the cells closely mimics the structure of our bones. This can provide comparable strength-to-weight ratios to bone, and provides for better osteointegration (the ability of bone to grow into the implant), resulting in better performance and quicker recovery [26].

Lattice, mesh, and cellular structures are a simplified version of topology optimization, which consists of transforming a solid into a 'truss' structure. Most engineers intuitively understand that trusses are useful for increasing the rigidity or strength of a beam while reducing its weight [26].

4.2 Unit cell types:

As mentioned before, to build a lattice structure, unit cell has to be defined depending on the application and conditions of the surrounding environment. In order to define that, types of unit cell have to be known.

4.2.1 Graph unit cells:

There is a large collection of cell structures which are built to be repeated within the lattice. For a lattice structure to be fully defined, the unit cell must be precisely characterized in terms of the overall description of the structure design, generation method and intrinsic properties. Extensive studies concerning the different unit cells show that only a relatively small amount of lattice structures exist in the current time, of which some are slight variations of other existing cells [5].

In general, each cell type should in theory employ unique capabilities that make it superior to other cells in a certain way, such as increased energy absorption or relatively high strength to weight ratios. The most common cell structures include cubic, octet, hexagonal, diamond, face centered cubic and tetrahedron as shown in Figure 4.2 [5]. The strut diameters used in lattice structures must be of a diameter such that they can both be manufactured as well as provide the required mechanical properties to the part [26].

Figure 4.2 Different graph unit cell types for lattice structure [5]

4.2.2 Triply Periodic Minimal Surface (TPMS):

Triply periodic minimal surfaces are a particular subset of minimal surfaces which can continuously fill space in three perpendicular directions. Despite the fact that they are difficult to fabricate with traditional methods, TPMS are readily manufacturable with additive manufacturing technologies. Applications of TPMS

structures with additive manufacturing aim for high-value products, including porous bio-implants, energy absorbing structures and thermal systems [27].

TPMS come in various structures, of which the most commonly used are Schwarz (P, D & H), Schoen's Gyroid, Schoen's I-WP and Schoen's D. Figure 4.3 shows the different topologies of TPMS unit cells.

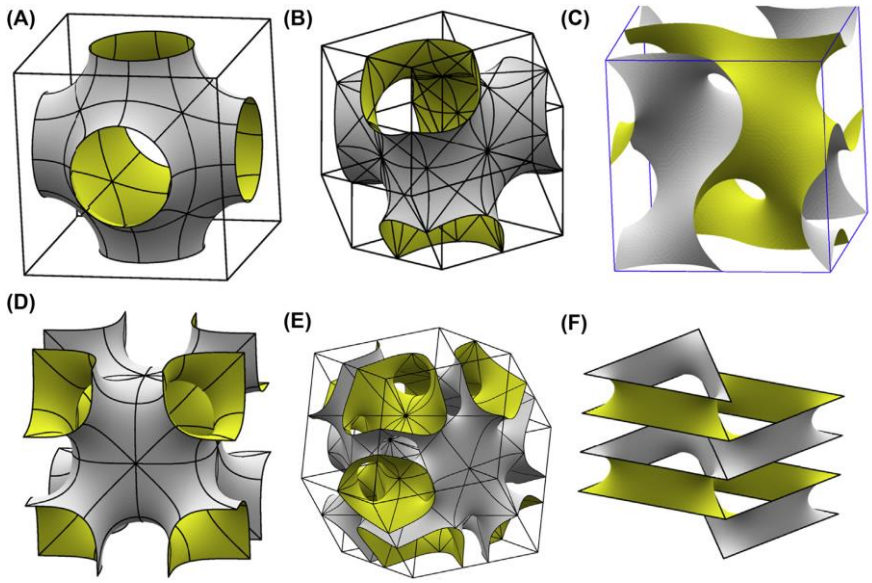

Figure 4.3 TPMS unit cells. (A) Schwarz' P Surface cubic unit cell, (B) Schwarz' D Surface rhombic dodecahedron unit cell, (C) Schoen's Gyroid Surface cubic unit cell, (D) Schoen's I-WP surface, (E) Schoen's Complementary D Surface with rhombic dodecahedral unit cell, (F) Schwarz' H Surface with triangular prism unit cell [27]

The Diamond (D), Gyroid (G) and Primitive (P) surfaces have cubic crystalline symmetry, and have been shown to be approximated by level-set equations in local Cartesian coordinates, X, Y, Z, according to a specified iso-value, t (as given in the following equations). The fundamental D, G, and P surfaces correspond to an iso-value of zero [27].

$$\cos(Z)\sin(X+Y)+\sin(Z)\cos(X-Y)=t \quad \text{Diamond (D) surface (1)}$$

$$\sin(X)\cos(Y)+\sin(Y)\cos(Z)+\sin(Z)\cos(X)=t \quad \text{Gyroid (G) surface (2)}$$

$$\cos(X)+\cos(Y)+\cos(Z)=t \quad \text{Primitive (P) surface (3)}$$

4.2.2.1 Gyroid unit cell:

Of the known TPMS permutations, the Gyroid, identified by Schoen in 1970 has captured much engineering interest due to its remarkable geometric characteristics and mechanical properties. Figure 4.4 shows a block og lattice structure of Gyroid unit cell [27].

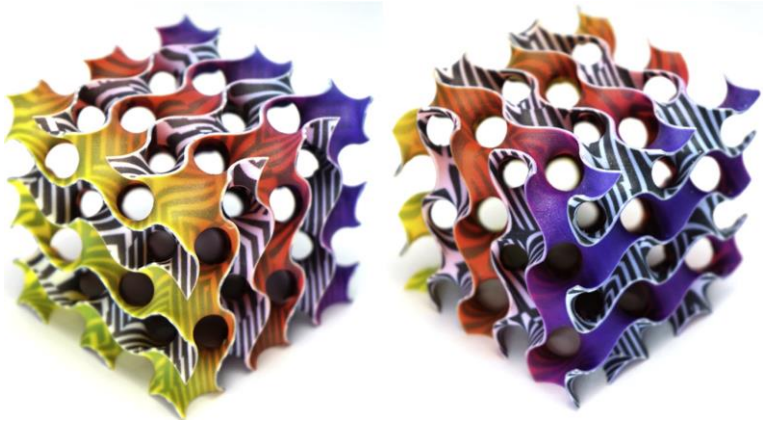

Figure 4.4 AM technology to show the complexity of the TPMS gyroid structure [27]

The Gyroid has no reflection symmetry or linear features, enabling the mitigation of stress concentrations when subject to mechanical loading: this outcome is particularly important for weak-link failure modes such as fatigue. Gyroid is preferred due to its robust manufacturability and exceptional mechanical properties. This gyroid can be fabricated by continuous curvilinear tool paths and is therefore compatible with many AM technologies, including metallic, ceramic and polymer structures [27].

4.2.2.2 Schwarz P unit cell:

Schoen named this surface 'primitive' because it has two intertwined congruent labyrinths, each with the shape of an inflated tubular version of the simple cubic lattice. While the standard P surface has cubic symmetry, the unit cell can be any rectangular box, producing a family of minimal surfaces with the same topology [28]. Figure 4.5 shows an illustration of Schwarz P unit cell. The P surface has been considered for prototyping tissue scaffolds with a high surface-to-volume ratio and porosity [29].

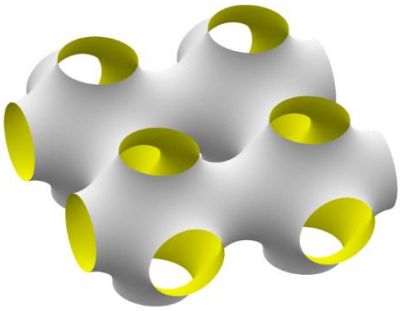

Figure 4.5 Schwarz P unit cell

Since the previous core research [5] used the graph unit cells to design the custom-made insole, this study will continue the approach using these two topologies of TPMS, due to their highly valuable properties and capabilities of shock absorption.

4.3 Thermoplastic material (TPU):

This study proposes a new design of the custom-made insole with lattice structure of TPMS unit cells, and also using another method of additive manufacturing, which is fused deposition modeling (FDM). This technique utilizes a thermoplastic filament where it heats the material to a degree of melting, then the extruder moves according to a pre-programmed code in order to build the layers of the part. Thermoplastic materials are quiet variant; the most commonly used thermoplastics with FDM are Acrylonitrile butadiene styrene (ABS) and Polylactic acid (PLA). They are very strong mechanically but they do not have the advantage of flexibility, which is extremely required in the application of medical insoles to deliver the maximum comfort to the patient.

Therefore, depending on previous research of the perfect material to be used in insoles manufacturing (as mentioned in Chapter 3), thermoplastic polyurethane (TPU) was chosen for this study.

TPU is a flexible, abrasion resistant thermoplastic. In certain blends, it can become very soft, but it still offers plenty of benefits and features. 3D printed parts with TPU

are durable and have the ability to withstand temperatures that may reach to 80° degrees. Table 4.1 shows the specifications for TPU filament used in FDM [34].

Table 4.1 Specifications of TPU [34]

Features	
Durability	*High*
Strength	*High*
Flexibility	*Very high*
Resistance	
Abrasion resistance	*High*
Chemical resistance	*Medium high*
Water resistance	*Medium*
Temperatures	
Nozzle temperature	*220 - 250° C*
Heated bed	*Up to 60°*

4.4 Fatigue properties:

One of the main mechanical issues to consider while designing such a piece that will go under continuous loading of force is the fatigue properties, which means the behavior of the part after several cycles of loading. This section will discuss the fatigue properties of the used material (TPU), as well as the fatigue of the selected unit cell (Gyroid).

4.4.1 Fatigue properties of TPU:

Several studies have tested the fatigue properties of TPU in different applications, although test on footwear and medical insoles are very few to not existent. J. Wang et al. defined TPU as linear segmented block polymers that are prone to microphase separation due to the thermodynamic incompatibility between polar hard segments and relatively nonpolar soft segments [30]. The hard segments of TPU (HS) brings the feature of good mechanical strength, while the soft segments (SS) provide the flexibility and elastic behavior. Therefore, the material

can be modified and customized by setting the ration of hard segments to soft segments with the structural morphologies, which enhances the performance in regards to the application of interest [30].

In another detailed study that was carried out by Z. Major et al. [31], the research team aimed to characterize the fatigue behavior of TPU, since the parts that are made with this material are frequently exposed to complex combination of loads, which may result in failure and damage of these parts. However, unlike classic elastomers, only physical cross-links exist in this material and may be destroyed at high temperatures. Since TPU has almost two kinds of behavior; elastomer-like and thermoplastic-like, the fracture behavior can be characterized in terms of the tearing energy concept (T) and the fracture toughness (K) or critical strain energy release rate (G) [31].

To study this behavior, they used two models of TPU material; one is unfilled neat TPU (TPU2un) and the other is filled TPU (TPU4g) by filler typically applied for tribological applications. These materials were made into specimens of faint waist pure shear (FWPS) with 2 mm nominal thickness. The specimens were then subjected to displacement-controlled fatigue tests at frequencies of 2 and 10 Hz. The crack length was measured at the end of the predefined cycle number of 40, 400 and 4000 cycles for every test amplitude [31].

In conclusion to their study and experiment, there was no significant difference between unfilled and filled TPU at a frequency of 2 Hz and cycle number of 4000, although unfilled TPU showed a better performance of crack resistance at a frequency of 10 Hz. The test was set with two different frequencies because thermoplastic elastomers tend to be more sensitive to frequency. Moreover, at the frequency of 2 Hz, only stable crack growth was observed, while at 10 Hz, crack instability has obviously occurred. For both models of TPU, increasing the cycles number led to a small decrease in the tearing energy (T) [31]. Figure 4.6 shows the curves of crack growth behavior with the increase of cycles number for both unfilled and filled TPU, with a focus on the area of instability at the frequency of 10 Hz.

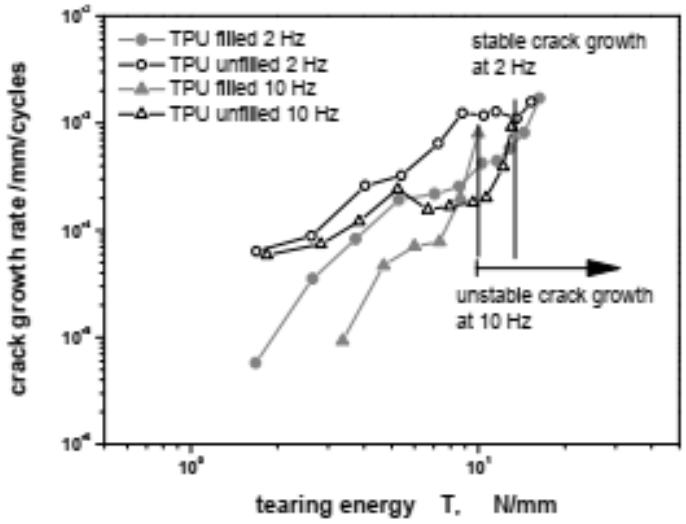

Figure 4.6 Comparison of the fatigue crack growth curves at 2 and 10 Hz for unfilled TPU [31]

4.4.2 Fatigue properties of Gyroid unit cell:

There was a unique research by D. W. Abueidda et al. [32] that aimed to study the mechanical properties of 3D printed polymeric Gyroid cellular structure. They fabricated Gyroid-structure specimens using selective laser sintering (SLS) technique. The specimens were cubes of four-unit cells per side length, resulting in a 4x4x4 configuration, made of Polyamide 12 based thermal plastic. The density of Gyroid lattice ranged between 7% and 46% in the 3D printed specimens [32].

The mechanical behavior of the Gyroid-structures was investigated both computationally and experimentally. Samples were tested under compression at room temperature at an applied strain rate of 0.01 S^{-1}. Figure 4.7 shows the stress-strain curves of the tested samples of various densities, both is horizontal and vertical orientations.

The stress-strain curves begin with a linear elastic behavior after which stress nonlinearly increases with the applied strain. The slopes of the stress-strain curves continue to taper until the slopes are diminished, and the strengths of the Gyroid-structure are achieved. After that, stress enter a softening region and decline in value. For the higher relative densities of 30.5%, 36%, 40%, and 46%, the softening behavior has a negative slope with a low-value magnitude and continues

until all layers of the sample are collapsed, after which the sample exhibits densification. In contrast, both 7% and 14% densities show more significant softening behavior which is then followed by an oscillation of hardening and softening behaviors until densification [32].

In conclusion, higher levels of density of Gyroid-structure lattice guaranteed a better softening effect, higher strength in terms of MPa force, higher levels of stress to withstand and higher absorption of energy [32].

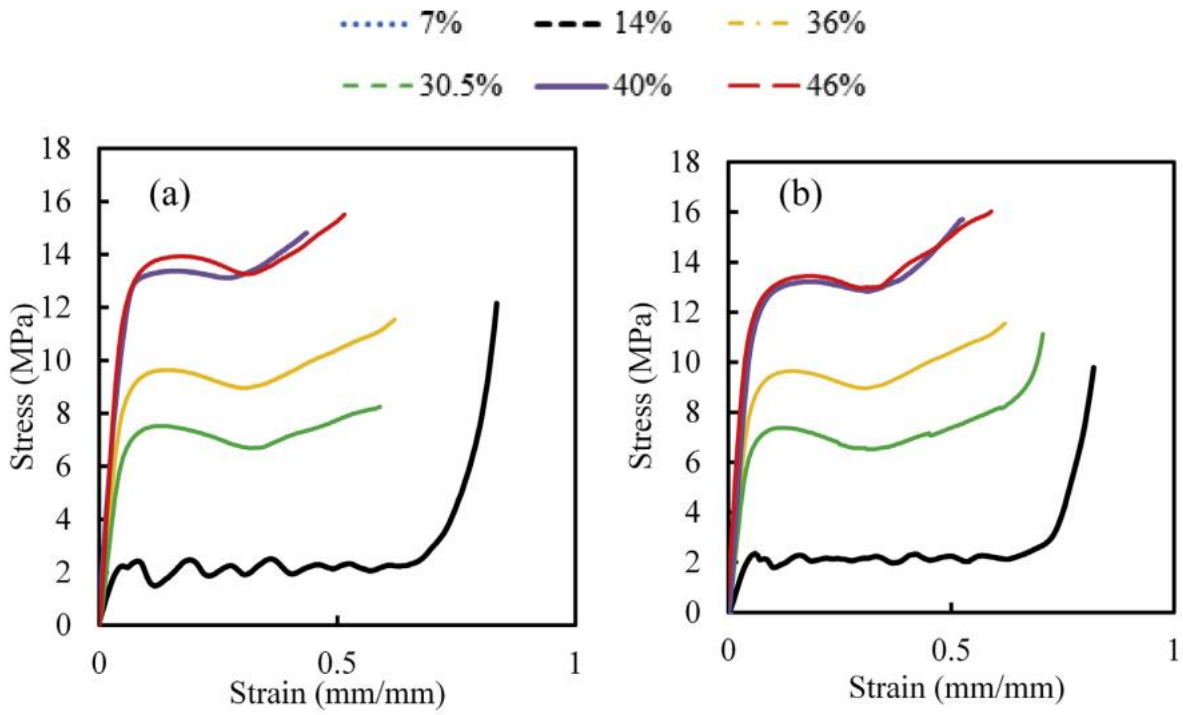

Figure 4.7 stress-strain curves of the Gyroid-structures at different relative densities. a) horizontal orientation with respect to the 3D printed layers, b) vertical orientation with respect to the 3D printed layers [32]

Chapter 5:

Case Study

Chapter introduction:

Gathering all the resources from previous chapters, here starts the real work of designing a custom-made insole. This chapter will elaborate on the practical steps that were taken into account to carry out the design process. Lattice structure, specific unit cell type, thickness and density, proper material and loading forces; all of these elements involved in designing the insole through the following phases.

5.1 Creating TPMS specimens:

In order to define the best geometry of the unit cell that can be used to design a comfortable insole, specimens have to be created and subjected to simulation (finite element analysis) and compression tests, thus their mechanical response can be revealed. Using the phenomenal software (nTopology), boxes were created of various dimensions. The general trend of dimension is 32mm x 32mm x L, where L equals to the cell size + 2mm as the plates' height, as shown in Figure 5.1. The width of the plates was prone to modification as to fit the cell size, to have a complete set of cells within the box.

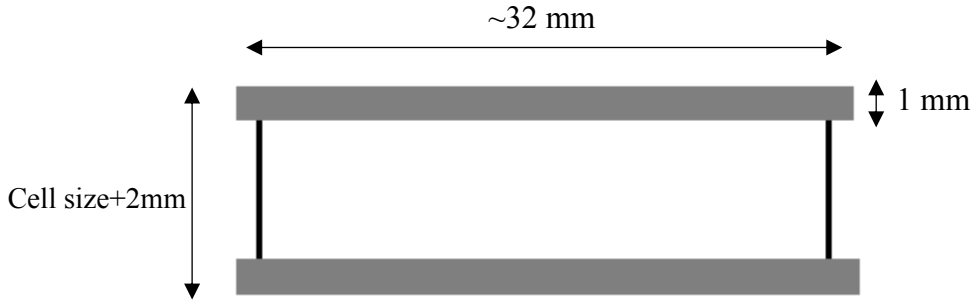

Figure 5.1 General shape of the specimens

The unit cell types to be used were chosen as Gyroid unit cell and Schwarz P unit cell. As previously mentioned in the chapters of this study, these two topologies have the advantage of shock absorbance and strong mechanical robustness. To build a lattice structure of these unit cells in nTopology, two basic values must be set in millimeters: the cell size which means the uniform dimension of a box that holds the cell, and the strut diameter which means thickness of the cylinder that is responsible for forming the topology.

After testing several values and combinations of cell sizes with strut diameters, it was observed that at a certain ratio of strut diameter to cell size, the unit cell loses its shape and it deforms into another shape, which might affect its mechanical properties. As for Gyroid unit cell, strut diameter should not be more than 25% of the cell size, while for Schwarz P, strut diameter should not be more than 20% of the cell size. Figure 5.2 shows the normal shape of Gyroid and Schwarz P, and the deformed shape of the cells when exceeding these ratios.

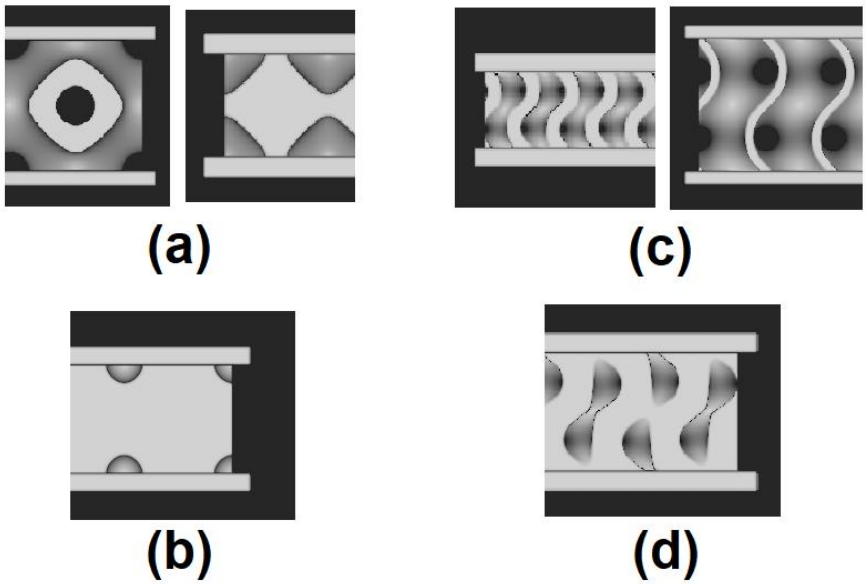

Figure 5.2 TPMS unit cells from nTopology. a) Acceptable Schwarz P at low and high densities, b) Deformed Schwarz P with high strut diameter, c) Acceptable Gyroid cell at high and low densities, d) deformed Gyroid with high strut diameter

Upon this observation, 11 specimens with Gyroid lattice and 16 specimens with Schwarz P lattice were created in nTopology, with the dimensions that are listed in Table 5.1.

The other input to be set in nTopology to create lattice structure is the cell map, which is the volume that is required to contain the lattice. Cell map divides the volume of the part into boxes of dimensions (x, y, z) that will embrace the unit sell of the lattice. Therefore, these dimensions should always match the selected cell size. Sometimes, the position of the cell map should be modified to match the coordination of the original box as a whole.

Table 5.1 Dimensions of the created TPMS specimens in nTopology

Gyroid		Schwarz P	
Cell size (mm)	**Strut diameter (mm)**	**Cell size (mm)**	**Strut diameter (mm)**
12	2.5	10	3
12	1	10	2
10	2	10	2
10	1	10	1
8	2	8	2
8	1	8	1
6	1.5	6	1.5
6	1	6	1.2
5	1	6	0.8
4	1	6	0.5
2	0.5	5	1
		5	0.5
		4	1
		4	0.8
		4	0.5
		2	0.4

5.2 Finite element analysis:

Finite Element Analysis simulates the physical phenomena using mathematical numerical techniques by discretizing them into small elements. This helps predict the mechanical response of the lattice structure under certain boundary conditions such as the plantar pressure and shear force, which are of interest in the application of this study. Hence, to run a finite element static analysis, certain steps have to be followed, starting from building a finite element model to observing the results.

5.2.1 Finite element model:

An FE model brings together all of the necessary elements for the part to be analyzed, whether in simulation, optimization, or further analysis. An FE model is built up of Components and Connectors. Each component contains an FE Mesh and Attributes, while connectors are made up of Tie Constraints, Structural Bonded Contacts, or Thermal Bonded Contacts that allow the analysis of multiple

FE Components [35]. Therefore, after building lattice boxes (specimens) as previously mentioned, FE mesh were created as solid mesh from the volume mesh of each specimen. On the other hand, attributes were taken as the isotropic material properties that are identified by Young Modulus and Poisson ratio of the 3D printing material, hence TPU filament. These values were set from TPU datasheet as 18 MPa and 0.4, respectively. Afterwards, FE mesh together with solid attributes were the input of the FE model block in nTopology that is required for the FE analysis.

5.2.2 Boundary conditions:

Since FE analysis simulates the physical phenomena which is the response of lattice structure under certain conditions, these conditions must be defined with the so-called "boundary conditions". In FEA, boundary conditions can be as many as needed. In this study, there are only two forces that impact on the foot movement: plantar pressure and shear stress. In addition to these forces, a displacement restraint must always be defined as the static side of the body, which can be represented here by the ground reaction force, considering the foot to be fixed on the ground,

As previously mentioned, plantar pressure is the normal pressure upon the foot on the vertical axis of the space. The average value of plantar pressure was selected as of 150 kPa, although medical references suggest that it might reach to 350 kPa in certain medical cases, but the size of the specimens is more likely to collapse at such high values of pressure. For that reason, 150 kPa of normal pressure was chosen as the first boundary condition.

The second boundary condition is shear stress, the horizontal force that has an impact on the foot movement. The average value of shear stress was selected as of 61 N. Finally, displacement restraint does not require any specific values, except for the coordinates of the fixed surface. Figure 5.3 shows the boundary conditions of the FE analysis that was achieved in nTopology.

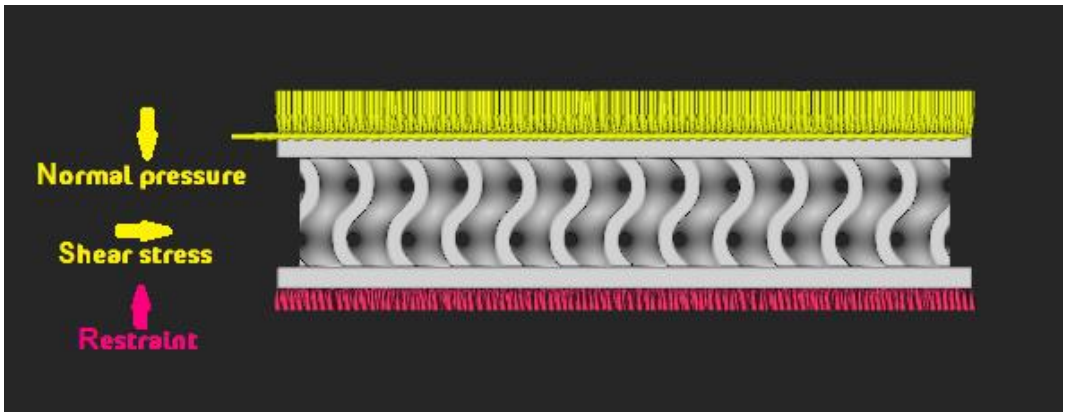

Figure 5.3 Boundary conditions of FEA in one of the Gyroid-structure specimens

After setting all the required components of FE analysis, the results are shown as visualizations of displacement, strain, stress and reaction forces. For the purpose of this study, only displacement and Von Mises stress were important for the observation.

5.3 Compression tests:

Before heading towards the design of the full insole, specimens should go under compression tests in order to define the best combination of cell size and strut diameter to be used in the insole. However, this study is a continuation of the research that was carried out by R. Simone [5] in the first place, hence it works on the future goals of it as a priority. One of the goals was to test the graph unit cells' specimens that were created in the same way as the TPMS specimens were created, and were 3D printed with TPU using SLS technique. In addition, EVA samples were fetched from a local company that manufactures prefabricated insoles from EVA foam. EVA samples were 7 pieces graduating in stiffness as a scale of 1 (stiffest) to 7 (softest), with a surface area of ~900 mm^2 and different height as shown in Figure 5.4.

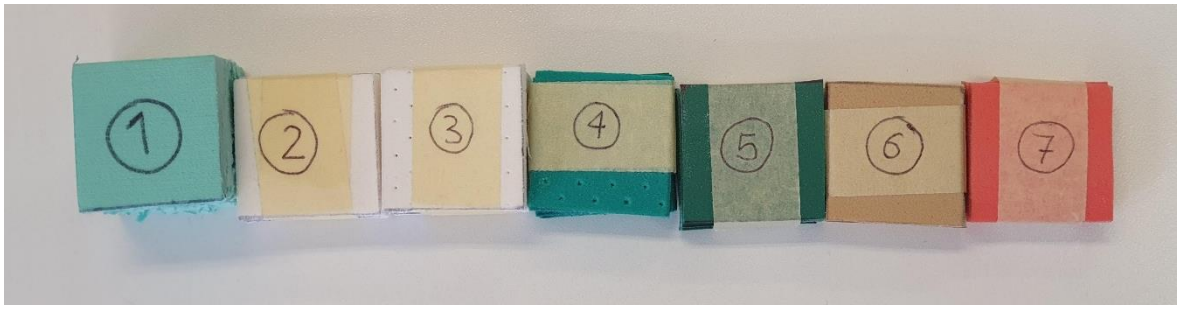

Figure 5.4 EVA samples to be tested under compression (1: hardest, 7: softest)

Compression tests were carried out in the laboratory of the department of Industrial Engineering and Mathematical Sciences at Universitá Politecnica delle Marche. The tests were displacement-controlled in terms of millimeters per second. Usually in the prefabricated insoles, the lower section which mostly occupies the back of the foot is made of stiff EVA foam (from 1 to 4 in Figure 5.4), while the upper and front section is made of soft EVA (from 5 to 7 in Figure 5.4). Based on that information, tests were made to compare the Young Modulus (i.e., the elasticity modulus) of both EVA and TPU SLS specimens in order to define the most resembling topology of lattice structure to EVA prefabricated insole. In total, 7 tests were carried out on EVA foam and 10 tests were carried out on TPU SLS specimens (4 Octet, 3 Fluorite, 3 Face center cubic). Figure 5.5 shows some of the specimens from the compression test in the lab.

Figure 5.5 EVA foam and TPU SLS specimens in the compression test

5.4 Foot scan and pressure map:

A scan of the foot was taken from a healthy male subject at the insoles company and it was generated as CAD file to be modified (if necessary) in Rhino 6 and utilized in the design afterwards. Figure 5.6 shows the CAD file of the insole based on the foot scan. The same subject has done a plantar pressure recording session before, and his pedobarographic image was fetched as shown in Figure 5.7. The image was imported into Rhino 6 and converted to CSV file (points and coordinates) to be later

used as point map in nTopology, for the purpose of designing the insole which will be explained in the next section.

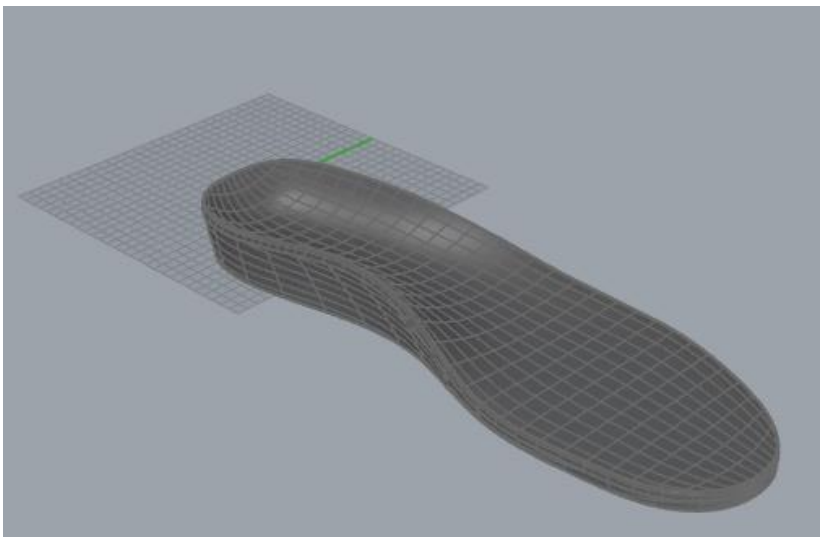

Figure 5.6 CAD file of the insole based on the foot scan

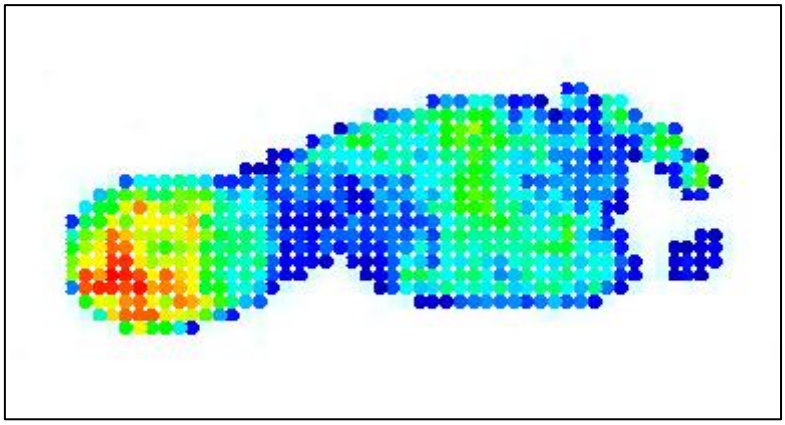

Figure 5.7 Pedobarographic image (pressure map) of the left foot

5.5 Full insole design:

After collecting the results of FEA for TPMS specimens and compression tests for TPU SLS specimens, and with the utilization of the CAD file and the pressure map, two full insoles with lattice structures were designed in nTopology.

Two methods were used to generate the lattice structures of both insoles. Regarding the insole with graph unit cell lattice, volume lattice was first generated from the volume of the insole. Then, ramp was generated from the pressure map (scalar point map field) as to grade the strut diameter while keeping the cell size

constant, via “Thicken Body” block which changes the dimensions of a body using a scalar field such as the ramp. On the other hand, regarding the insole with TPMS lattice, periodic lattice body was generated from the warped cell map, which is the original cell map of the body but warped according to the pressure map, in a way that grades the cell size while keeping the strut diameter constant.

The full insole with graph unit cell lattice was designed with open sides because it will be 3D printed using SLS technique, which requires a complicated post-printing process of cleaning the excessive powder. However, to unify the shape and characteristics of both insoles for further experimentation, the other insole with TPMS lattice was also designed with open sides. This provides better visualization for the assessment as well. Moreover, a pair of traditional customized EVA insoles for the left and right feet were fetched from the company. Therefore, at the end of this trial, there will be three types of insoles to try: customized EVA foam, customized TPU SLS with graph unit cell lattice and customized TPU FDM with TPMS lattice.

Chapter 6:

Results & Discussion

Chapter introduction:

This chapter demonstrates explicitly all the results of what was carried out in the previous chapter, hence finite element analysis, compression tests and the full insole design.

6.1 Results:

6.1.1 Finite element analysis:

As explained in the previous chapter, FE model was created from each specimen using nTopology software, then analyzed under certain boundary conditions (plantar pressure, shear stress, displacement restraint). Observations from the analysis involved the displacement on both directions; X axis for the effect of shear stress (horizontal) and Z axis for the effect of the plantar pressure (vertical). Moreover, Von Mises stress was observed as an additional parameter for evaluation. Displacement components were observed using the field view at the center of the plate surface, as shown in Figure 6.1 for an example, while Von Mises stress was taken as the maximum value throughout the body.

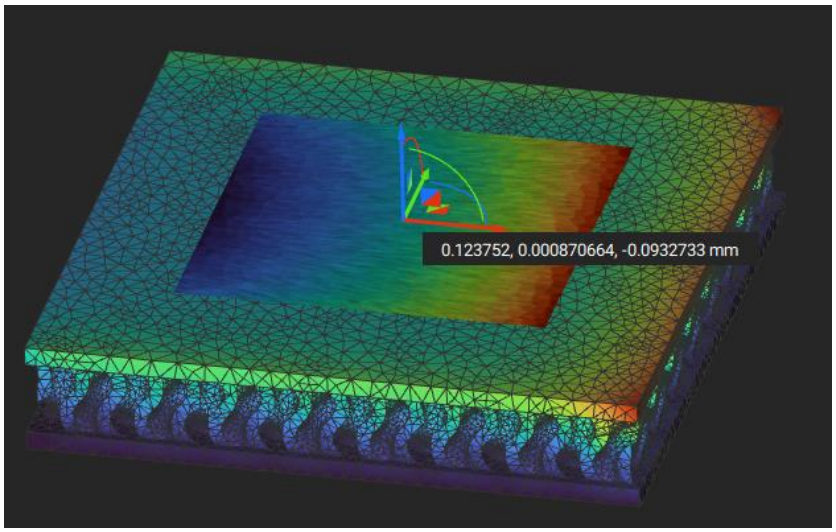

Figure 6.1 An example of observed displacement at the center of the plate (4 mm x1 mm Gyroid specimen)

In total, 11 specimens with Gyroid lattice and 16 specimens with Schwarz P lattice were analyzed in FEA. Cell size ranged from 2 mm to 10 mm, to consider the applicable range of thickness for regular foot insoles. Density was calculated

as the ratio of the lattice volume to the total box volume in terms of percentage value. Horizontal deformation was calculated as the ratio of the horizontal displacement to the specimen width. Vertical deformation was calculated as the ratio of the vertical displacement to the specimen height. Vertical stiffness which should resemble the Young modulus (elasticity) was calculated as the resultant of dividing the normal pressure by the vertical deformation. The value of vertical stiffness was the essential value to consider in the comparison with EVA foam. Table 6.1 shows the abovementioned values for all TPMS specimens in this study. For detailed results, please see the Appendix.

Table 6.1 FEA results of the specimens with Gyroid and Schwarz P lattice

Unit cell type	Cell size (mm)	Strut diameter (mm)	Density	Horizontal displacement (mm)	Vertical displacement (mm)	Vertical deformation	Horizontal deformation	Vertical stiffness [MPa]	Horizontal stiffness [MPa]	Von mises stress (Pa)
Gyroid	12	2.5	33%	0.45	0.38	3%	1%	5.53	3.66	2.24E+06
Gyroid	12	1	13%	1.49	1.19	9%	4%	1.76	1.11	6.97E+06
Gyroid	10	2	29%	0.54	0.32	3%	2%	5.63	3.53	3.12E+06
Gyroid	10	1	14%	1.37	0.77	6%	4%	2.34	1.39	7.02E+06
Gyroid	8	2	37%	0.26	0.17	2%	1%	8.82	7.11	3.20E+06
Gyroid	8	1	18%	0.65	0.43	4%	2%	3.49	2.84	5.09E+06
Gyroid	6	1.5	32%	0.21	0.13	2%	1%	9.23	9.08	2.27E+06
Gyroid	6	1	21%	0.35	0.23	3%	1%	5.22	5.45	3.60E+06
Gyroid	5	1	24%	0.24	0.16	2%	1%	6.56	7.94	3.48E+06
Gyroid	4	1	31%	0.12	0.09	2%	0%	10.00	15.40	1.62E+06
Gyroid	2	0.5	29%	0.06	0.03	1%	0%	16.00	32.80	1.92E+06
Schwarz	10	3	62%	0.18	0.09	1%	1%	20.00	10.59	2.02E+06
Schwarz	10	2	49%	0.26	0.14	1%	1%	12.86	7.33	6.25E+06
Schwarz	10	2	45%	0.27	0.15	1%	1%	13.00	7.06	1.72E+07
Schwarz	10	1	25%	0.73	0.42	4%	2%	4.29	2.61	4.13E+06
Schwarz	8	2	58%	0.15	0.18	2%	0%	8.33	12.32	1.64E+06
Schwarz	8	1	32%	0.35	0.46	5%	1%	3.26	5.28	2.34E+06
Schwarz	6	1.5	50%	0.11	0.06	1%	0%	20.00	17.33	967980
Schwarz	6	1.2	44%	0.14	0.08	1%	0%	15.00	13.62	1.38E+06
Schwarz	6	0.8	30%	0.23	0.14	2%	1%	8.57	8.29	2.61E+06
Schwarz	6	0.5	19%	0.43	0.28	4%	1%	4.29	4.43	3.50E+06
Schwarz	5	1	42%	0.11	0.09	1%	0%	11.67	17.33	1.97E+06
Schwarz	5	0.5	22%	0.26	0.21	3%	1%	5.00	7.33	1.60E+07
Schwarz	4	1	48%	0.07	0.05	1%	0%	18.00	26.41	1.66E+06
Schwarz	4	0.8	42%	0.08	0.07	1%	0%	12.86	23.11	2.10E+06
Schwarz	4	0.5	27%	0.15	0.14	2%	0%	6.43	12.32	3.13E+06
Schwarz	2	0.4	34%	0.04	0.02	1%	0%	24.00	46.21	3.24E+06

6.1.2 Compression tests:

Compression tests were conducted in two parts: the first part tested the EVA specimens (hard and soft) and the second part tested the TPU SLS specimens that previously showed values of density and vertical stiffness in FEA in nTopology as listed in Table 6.2. As the table lists, 4 Octet, 3 Fluorite and 3 Face center cubic specimens were tested under compression. The last column contains the empirical values of Young Modulus of the specimens from the tests.

Table 6.2 Virtual and empirical values of vertical stiffness and vertical of TPU SLS specimens

Unit cell type	Cell size (mm)	Struct diameter (mm)	Density	Vertical stiffness nTopology [MPa]	Vertical stiffness Compression test [MPa]
FCC	8	1	28%	2.00	0.02
FCC	12	2	29%	1.91	0.67
FCC	7.5	1.5	41%	6.48	1.07
Fluorite	8	1	31%	2.83	0.19
Fluorite	12	2	33%	5.12	0.85
Fluorite	7.5	1.5	46%	10.96	2.17
Octet	18	1.5	19%	1.27	0.12
Octet	18	2	23%	2.42	0.62
Octet	12	2	39%	7.78	2.12
Octet	7	1	41%	6.75	0.59

In order to decide which topology of the abovementioned lattice structures is the best for using in the custom-made insole, EVA specimens were also tested under the same conditions of compression. Table 6.3 shows the values of Young Modulus of each EVA specimen as calculated from the stress-strain curve of the compression test, considering the density as 100% for all the pieces.

Table 6.3 Dimensions and Young Modulus of EVA specimens

Unit cell type	Height (mm)	Surface area (mm^2)	Density	Vertical stiffness Compression test [MPa]
EVA	30	900	100%	5.45
EVA	15	900	100%	3.28
EVA	20	900	100%	2.33
EVA	11	900	100%	1.34
EVA	12	900	100%	0.77
EVA	13	900	100%	0.89
EVA	12	900	100%	0.23

To understand the behavior of both types of specimens, values were taken from the reaction force-displacement curve that resulted from the compression test in the lab. After some analysis and calculations, these curves were converted into stress-strain curves. Figure 6.2 shows the stress-strain curves for hard soft specimens of EVA foam, and Figure 6.3 shows the stress-strain curves for soft specimens of EVA foam.

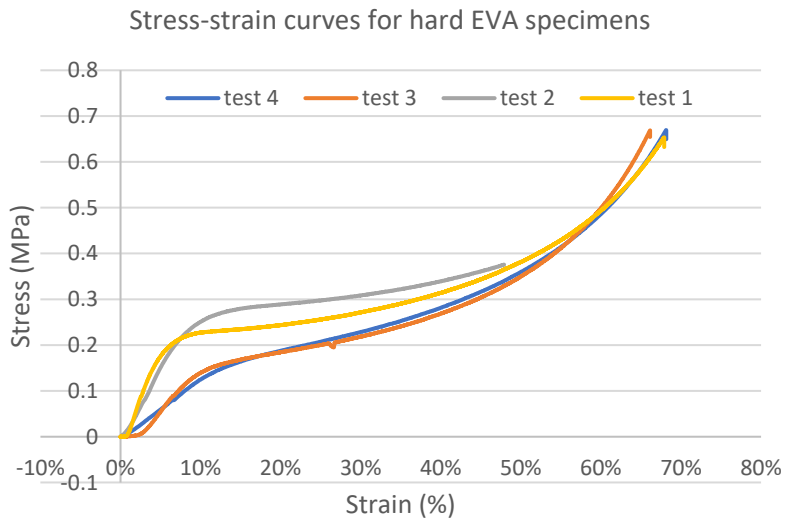

Figure 6.2 Stress-strain curves of hard EVA specimens (1: hardest, 4 least hard)

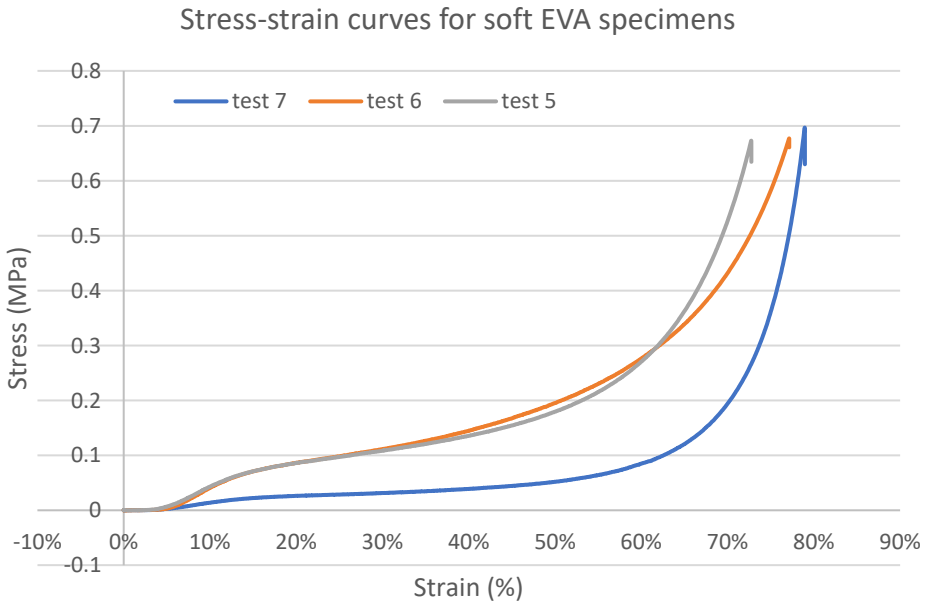

Figure 6.3 Stress-strain curves of soft EVA specimens (7: softest, 5: least soft)

On the other hand, to understand the different behavior of each unit cell under compression, values of the tests were taken and converted to stress-strain curves in the same manner. Figure 6.4 shows the stress-strain curves for Octet, Fluorite and FCC unit cells with different combinations of cell size and strut diameter.

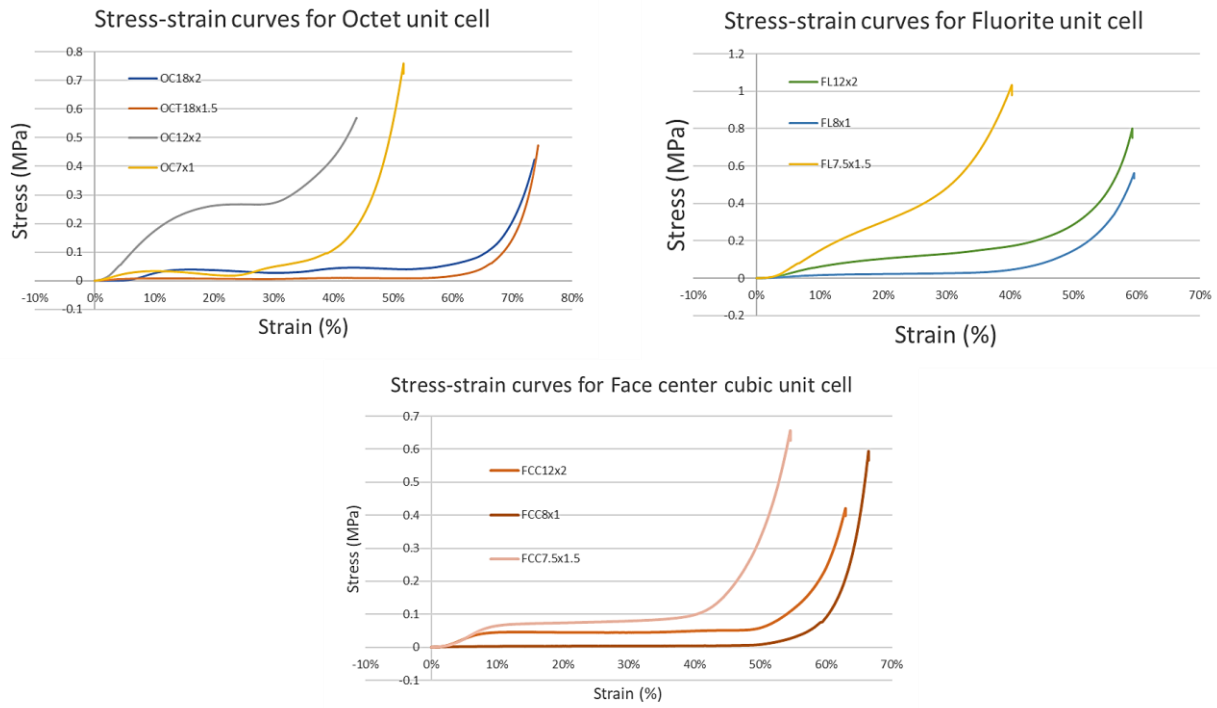

Figure 6.4 Stress-strain curves for three types of unit cell (Octet, Fluorite, FCC)

6.1.3 Full insole design:

As mentioned in the previous chapter, a CAD file of the insole body based on the foot scan was fetched. It was modified in Rhino 6 where 3 mm were added to the insole body to increase the thickness, allowing more organized lattice structure within for both types. The pressure map was utilized in generating a ramp field that grades a value and maintains the other as the following:

6.1.3.1 Full insole with Fluorite-lattice structure:

In this version of lattice structure, a volume lattice is created and graded via the ramp. After analyzing the values from Table 6.2, the cell size was fixed at 7mm while the strut diameter has been graded from 2mm to 1mm for the lowest value of pressure to the highest value, respectively, as shown in Figure 6.5.

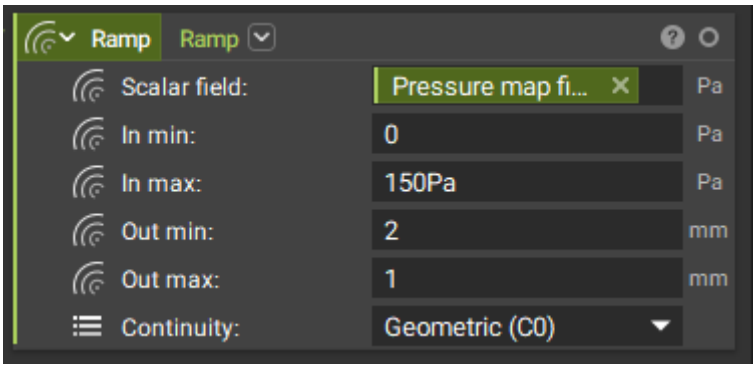

Figure 6.5 Ramp block for the Fluorite-lattice insole from nTopology

Afterwards, the resultant lattice was combined with the upper and lower surfaces of the insole CAD body, thus an open-sided insole with Fluorite-lattice structure was created, which is shown in Figure 6.6.

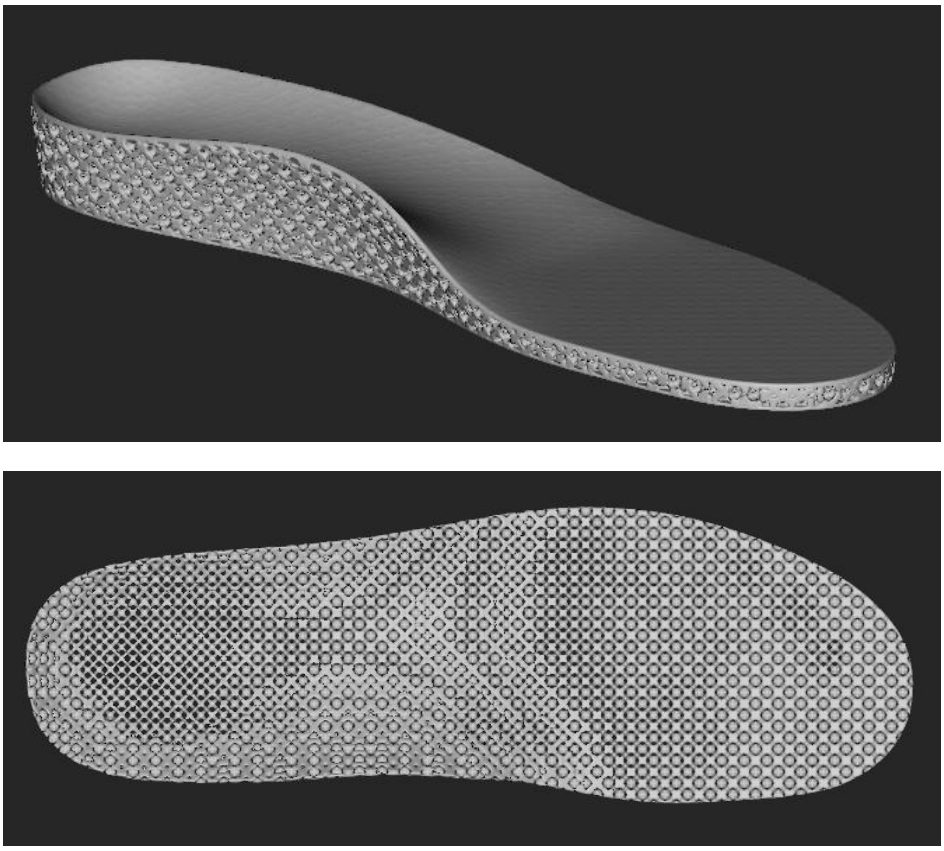

Figure 6.6 Graded insole with Fluorite-lattice structure (3D perspective and top view)

6.1.3.2 Full insole with Gyroid-lattice structure:

In this version of lattice structure, a periodic lattice body is created and graded via the ramp. After analyzing the data from Table 6.1, the most similar combinations of Gyroid dimensions (cell size x strut diameter) to hard and soft

EVA foam were 4mm x1mm and 12mm x 1mm, respectively. The first combination relates to low values of pressure, while the second one relates to high values of pressure. In other words, the ramp here graded the cell size while maintaining the strut diameter as a constant. Afterwards, the resultant lattice was combined with the upper and lower surfaces of the insole CAD body, thus an open-sided insole with Gyroid-lattice structure was created, which is shown in Figure 6.7.

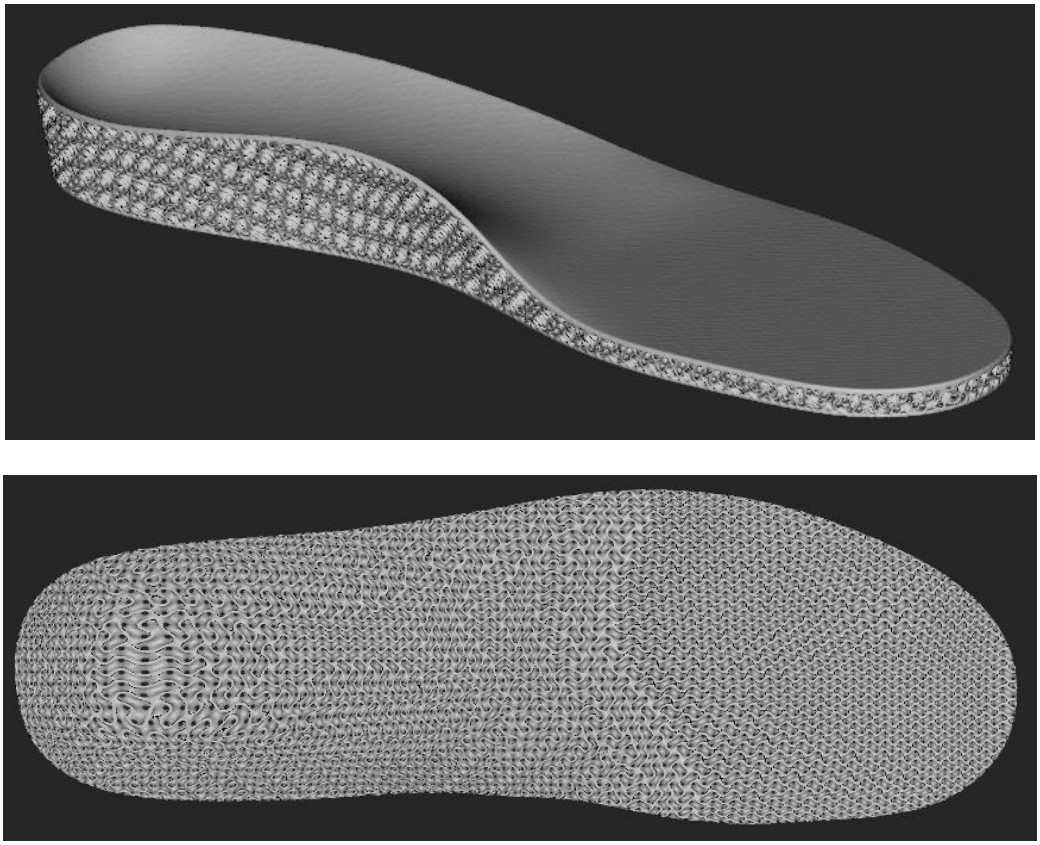

Figure 6.7 Graded insole with Gyroid-lattice structure (3D perspective and top view)

6.2 Discussion:

Specimens with TPMS lattice structure were created in nTopology and analyzed using the finite element analysis. During that process, the most important observation was that Gyroid topology has a more complex geometry than Schwarz P. The solid mesh block that was used in creating the FE model of Gyroid was different from the one that was used with Schwarz P due to that fact. However, Gyroid structure provided a wider range of normal densities (without deforming the unit shape) than

Schwarz P. The latter was highly sensitive to the change of strut diameter, thus only large cell sizes were applicable, which is not very useful in the application of medical insoles. With Gyroid, lower heights, i.e. small cell size, were allowed to form. This also gives small to medium densities in general. With Schwarz P, larger cell size was more compatible with various values of strut diameter, which leads to higher densities in general. Density of the lattice structure indicates to the yielded stiffness, and that is the most significant indicator to its eligibility to be used in the medical insole modeling. This helps accelerates the classification of the specimens to be tested and used in the analysis from the beginning.

In the finite element analysis, and looking at the results from Table 6.1, it is obvious that in general, the density of Gyroid lattice structure in all the specimens is low to medium due to the distinguished geometry of the unit cell, while the density of Schwarz P lattice structure in all the specimens is medium to high. This indicates that Gyroid unit cell extends its advantage to form softer textures, which makes it more preferable to apply in the insole design. Gyroid even allows for greater displacement than Schwarz P, which supports the fact that it can produce softer textures. These results lead to the fact that Schwarz P lattice is stiffer than Gyroid lattice which can be observed from the vertical stiffness column. Gyroid has a more flexible range of vertical stiffness which facilitates the comparison to EVA foam. From the datasheet of TPU filament, it is reported that both the yield compressive strength and the ultimate compressive strength equal to 2.6 MPa. Therefore, looking at Von Mises stress column, it is safe to say that the stress value in most of the specimens is within the acceptable range. In other words, the higher the density, the lower is Von Mises stress in most of the specimens. Nevertheless, this is the maximum value of the stress and it occurs in very small regions at the tips of the unit cell, thus the increased value can be neglected.

The compression tests were the most critical part of this study because the empirical values indicated to several problems and solutions at the same time. First and foremost from Table 6.2, there was a noticeable difference of Young Modulus of TPU SLS specimens between the virtual analysis in nTopology and the real

compression test. One possible reason is that some of the essential dimensions of the specimen were not precisely achieved in the 3D printing due to a flaw in the printing process or post-printing cleaning process. This caused an obvious instability in the stress-strain curve in the Octet lattice structures (Figure 6.4) as well, because of the variant dimensions among distances in the space between the cells. Figure 6.8 shows an example of superimposing the virtual mesh of Octet 10x1 specimen next to the real printed body of it, to clearly point out to the difference in dimensions.

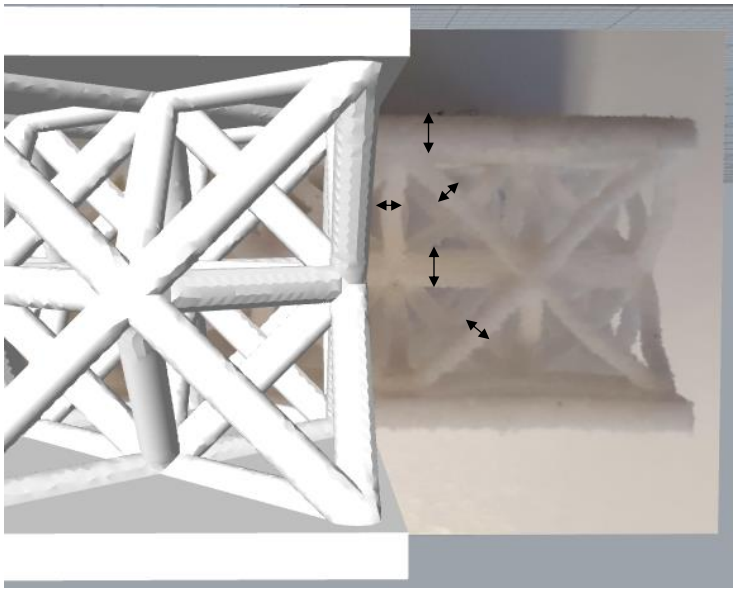

Figure 6.8 Superimposing Octet 10x1 mesh with Octet 10x1 printed body

This was the main reason of excluding Octet unit cell from the final list of candidates for modeling the insole. Moreover, looking at the stress-strain curves of FCC lattice structure in Figure 6.4, this unit cell always gives a short behavior of elasticity, even with low values of Young Modulus. This can be used in the application of extremely soft tissues, but definitely not in the application of medical insoles where there will be continuous loading of pressure in different regions of the foot. For that reason, it was also excluded from the candidate list. This leaves the Fluorite unit cell as the most feasible unit cell to be utilized in the lattice structure for the medical insole. To choose the best set of cell size and strut diameter, a comparison of Young Modulus was conducted between Fluorite specimens and EVA foam samples in order to choose the closet values to the hardest and softest EVA.

Eventually, Fluorite 7x2 mm (high density, stiff) was selected to confront low values of plantar pressure and Fluorite 7x1 mm (low density, soft) was selected to confront high values of plantar pressure, and that is exactly what was used in the ramp configuration as shown in Figure 6.5. The resultant geometry is highly complex which makes the conversion to mesh with high resolution and low tolerance a difficult process on the computer processor, therefore with the available capabilities, a mesh of the final insole with Fluorite lattice was created with tolerance value that equals to 1mm.

On another aspect, the values of Young Modulus of EVA foam samples were extremely useful in the determination of selecting the best combination of cell size and strut diameter of Gyroid lattice structures. After comparing EVA values to Gyroid virtual values from FEA in nTopology by the time of this study, with attention to maintaining the same strut diameter, Gyroid 4x1 mm (high density, stiff) was selected to confront low values of plantar pressure and Gyroid 12x1 mm (low density, soft) was selected to confront high values of plantar pressure, and that is exactly what was used in the ramp configuration as well as warping the cell map. As previously mentioned, Gyroid unit cell has a high complex geometry, which also makes it difficult to convert to mesh, especially within a medical insole. Hence, by the time of the study, a mesh of the final insole with Gyroid lattice was created with tolerance value that equals to 1mm.

6.3 Conclusion:

This research was devoted to combine previous knowledge with new aspects, in order to reach a new approach towards the custom design of medical insoles. The main goal was to achieve an acceptable level of expected comfort for the patient. Although, the insoles were not 3D printed by the time of this study and the overall satisfaction was not completely reached reached. However, the virtual results were reasonable and promising. Customized lattice structure in the entire insole was never proposed in research before, which makes this study and the one prior to it [5] novel concepts in the field of orthotics and foot insoles. The final designs are lightweight, elegant, ergonomic and beautifully shaped even on their own. The greatest difficulties

were having a good budget to cover all the expenses, knowing that a large number of specimens or modifications to the pre-designed ones might always be needed. In addition, the computing processes were most of the time highly complicated, thus they were conducted with the available devices. Nevertheless, the study resulted in very interesting outcomes using all available resources, which gives it the significance it deserves.

6.4 Future goals:

Scientific research cannot stop at a specific limit. Every day holds a new discovery and concept that can be used in every aspect. Therefore, future goals and continuation points to this study can be set as the following:

- Unit cells that construct a lattice can be self-engineered other than the unit cells that already exist. Furthermore, other types of unit cells can be tested for the same application.
- Instead of depending on a healthy subject, a specific disease can be targeted, e.g., diabetes.
- More than one lattice structure can be included in the same insole according to the pressure distribution over the foot.
- Looking for other software programs that can generate lattice structure with less CPU usage.
- Further compression tests, walking trials, fatigue tests can be carried out to evaluate the performance of the designed insoles.

References

[1] Z. Ma *et al.*, “Design and 3D printing of adjustable modulus porous structures for customized diabetic foot insoles,” *Int. J. Light. Mater. Manuf.*, vol. 2, no. 1, pp. 57–63, 2019.

[2] O. Ciobanu, Y. Soydan, and S. Hızal, “Customized Foot Orthosis Manufactured With 3D Printers,” *Proceeding IMS*, no. September, 2012.

[3] S. Jandova, R. Mendricky, and M. Jasurek, “Development of 3D printed insoles,” *Exp. Stress Anal. - 58th Int. Sci. Conf. EAN 2020*, no. June 2021, pp. 160–164, 2020.

[4] R. Teixeira *et al.*, “Towards customized footwear with improved comfort,” *Materials (Basel).*, vol. 14, no. 7, 2021.

[5] R. Simone, “Design of 3D printed custom-made orthopedic insoles”, Università Politecnica delle Marche, 2021.

[6] M. J. Hessert, M. Vyas, J. Leach, K. Hu, L. A. Lipsitz, and V. Novak, “Foot pressure distribution during walking in young and old adults,” *BMC Geriatr.*, vol. 5, pp. 1–8, 2005.

[7] N. Hayafune, Y. Hayafune, and H. A. C. Jacob, “Pressure and force distribution characteristics under the normal foot during the push-off phase in gait,” *Foot*, vol. 9, no. 2, pp. 88–92, 1999.

[8] S. S. Altayyar, “The importance of plantar pressure measurements and appropriate footwear for diabetic patients,” vol. 3, no. 3, pp. 21–24, 2016.

[9] L. Wafai, A. Zayegh, J. Woulfe, S. Mahfuzul, and R. Begg, “Identification of foot pathologies based on plantar pressure asymmetry,” *Sensors (Switzerland)*, vol. 15, no. 8, pp. 20392–20408, 2015.

[10] A. Amemiya *et al.*, “Shear Stress-Normal Stress (Pressure) Ratio Decides Forming Callus in Patients with Diabetic Neuropathy,” *J. Diabetes Res.*, vol. 2016, 2016.

[11] A. D. Jones, J. De Siqueira, J. E. Nixon, H. J. Siddle, P. R. Culmer, and D. A. Russell, “Plantar shear stress in the diabetic foot: A systematic review and meta-analysis,” *Diabet. Med.*, vol. 39, no. 1, pp. 1–15, 2022.

[12] S. Ndegwa and Charlene Argáez, “This report contains CADTH copyright material. It may be copied and used for non-commercial purposes, provided that attribution is given to CADTH.,” *Policy*, vol. 1, no. April, pp. 1–20, 2010.

[13] M. D'Amico *et al.*, "Data-driven CAD-CAM vs traditional total contact custom insoles: A novel quantitative-statistical framework for the evaluation of insoles offloading performance in diabetic foot," *PLoS One*, vol. 16, no. 3 March, pp. 1–20, 2021.

[14] R. Xu *et al.*, "Comparative study of the effects of customized 3D printed insole and prefabricated insole on plantar pressure and comfort in patients with symptomatic flatfoot," *Med. Sci. Monit.*, vol. 25, pp. 3510–3519, 2019.

[15] Cavanagh PR, Hewitt FG, Perry JE. In–shoe plantar pressure measurement: A review. The Foot. 1992;2 (4):185–194.

[16] Birke JA, Foto JG, Deepak S, et al. Measurement of pressure walking in footwear used in leprosy. Lepr Rev. 1994;65(3):262–271.

[17] Stephen FA, Lenore CC. Diabetic Foot Pressure Studies. Comparison Study of Patient–selected Shoes versus Clinician–selected Shoes. The Lower Extremity. 1994;1(1)

[18] Y. Meng, L. Yang, X. Jiang, B. István, and Y. Gu, "The effectiveness of personalized custom insoles on foot loading redistribution during walking and running," *J. Biomimetics, Biomater. Biomed. Eng.*, vol. 44, no. June, pp. 1–8, 2020.

[19] J. M. Gerrard, D. R. Bonanno, D. R. Bonanno, G. A. Whittaker, G. A. Whittaker, and K. B. Landorf, "Effect of different orthotic materials on plantar pressures: A systematic review," *J. Foot Ankle Res.*, vol. 13, no. 1, pp. 1–11, 2020.

[20] Healy A, Dunning DN, Chockalingam N. Effect of insole material on lower limb kinematics and plantar pressures during treadmill walking. Prosthetics Orthot Int. 2012;36(1):53–62

[21] McCormick CJ, Bonanno DR, Landorf KB. The effect of customised and sham foot orthoses on plantar pressures. J Foot Ankle Res. 2013;6:19

[22] Rao S, Baumhauer JF, Becica L, Nawoczenski DA. Shoe inserts alter plantar loading and function in patients with midfoot arthritis. J Orthop Sports Phys Ther. 2009;39(7):522–31

[23] Rogers K, Otter S, Birch I. The effect of PORON® and Plastazote® insoles on forefoot plantar pressures. Br J Podiatry. 2006;9(4):111–4

[24] Tong JW, Ng EY. Preliminary investigation on the reduction of plantar loading pressure with different insole materials (SRP–slow recovery Poron®, P–Poron®, PPF–Poron®+ Plastazote, firm and PPS–Poron®+ Plastazote, soft). Foot. 2010;20(1):1–6.

[25] E. Hermansson and E. Marcus, "A material study of insoles : Manufactured using different methods," p. 32, 2019.

[26] O. Diegel, A. Nordin, and D. Motte, *Additive Manufacturing Technologies BT - A Practical Guide to Design for Additive Manufacturing*. 2019.

[27] M. Leary, *Introduction to AM*. 2020.

[28] W. H. Meeks. "The theory of triply-periodic minimal surfaces". Indiana University Math. Journal, 39 (3):877-936, 1990.

[29] Jaemin Shin, Sungki Kim, Darae Jeong, Hyun Geun Lee, Dongsun Lee, Joong Yeon Lim, and Junseok Kim, "Finite Element Analysis of Schwarz P Surface Pore Geometries for Tissue-Engineered Scaffolds", Mathematical Problems in Engineering, Volume 2012, Article ID 694194

[30] J. Wang *et al.*, "Research of TPU materials for 3D printing aiming at non-pneumatic tires by FDM method," *Polymers (Basel).*, vol. 12, no. 11, pp. 1–19, 2020.

[31] Z. Major, M. Isasi, and T. Schwarz, "Characterization of the fracture and fatigue behavior of thermoplastic elastomer materials," *Key Eng. Mater.*, vol. 417–418, pp. 789–792, 2010.

[32] D. W. Abueidda, M. Elhebeary, C. S. (Andrew) Shiang, S. Pang, R. K. Abu Al-Rub, and I. M. Jasiuk, "Mechanical properties of 3D printed polymeric Gyroid cellular structures: Experimental and finite element study," *Mater. Des.*, vol. 165, no. March, p. 107597, 2019

[33] "Orthotics Guide", *Louisville Orthopaedic Clinic*.

[34] https://tractus3d.com/materials/tpu/

[35] nTopology Self-Guide, *nTopology*.

Appendix:

UNIT CELL TYPE	CELL SIZE (mm)	STRUT DIAMETER (mm)	DENSITY	PLATES HEIGHT (mm)	SPECIMEN HEIGHT WITH PLATES [mm]	SPECIMEN WIDTH [mm]	AREA [mm^2]	TOTAL VOLUME (mm^3)	LATTICE VOLUME (mm^3)
Gyroid	12	2.5	33%	1	14	37	1369	19166	6310.90
Gyroid	12	1	13%	1	14	37	1369	19166	2505.22
Gyroid	10	2	29%	1	12	32	1024	12288	3502.66
Gyroid	10	1	14%	1	12	32	1024	12288	1740.30
Gyroid	8	2	37%	1	10	33	1089	10890	4006.85
Gyroid	8	1	18%	1	10	33	1089	10890	1982.64
Gyroid	6	1.5	32%	1	8	32	1024	8192	2640.59
Gyroid	6	1	21%	1	8	32	1024	8192	1747.98
Gyroid	5	1	24%	1	7	32	1024	7168	1752.56
Gyroid	4	1	31%	1	6	33	1089	6534	2002.02
Gyroid	2	0.5	29%	0.6	3.2	31	961	3075.2	879.85
Schwarz	10	3	62%	1	12	32	1024	12288	7598.47
Schwarz	10	2	49%	1	12	32	1024	12288	5977.01
Schwarz	10	2	45%	1.5	13	32	1024	13312	5977.01
Schwarz	10	1	25%	1	12	32	1024	12288	3084.78
Schwarz	8	2	58%	1	10	33	1089	10890	6274.84
Schwarz	8	1	32%	1	10	33	1089	10890	3515.95
Schwarz	6	1.5	50%	1	8	32	1024	8192	4136.22
Schwarz	6	1.2	44%	1	8	32	1024	8192	3586.67
Schwarz	6	0.8	30%	1	8	32	1024	8192	2471.84
Schwarz	6	0.5	19%	1	8	32	1024	8192	1542.33
Schwarz	5	1	42%	1	7	32	1024	7168	2988.20
Schwarz	5	0.5	22%	1	7	32	1024	7168	1542.75
Schwarz	4	1	48%	1	6	33	1089	6534	3137.70
Schwarz	4	0.8	42%	1	6	33	1089	6534	2720.38
Schwarz	4	0.5	27%	1	6	33	1089	6534	1758.49
Schwarz	2	0.4	34%	0.6	3.2	33	1089	3484.8	1195.30

UNIT CELL TYPE	NORMAL PRESSURE (KPa)	SHEAR FORCE (N)	POISSON RATIO	YOUNG MODULUS (MPa)	HORIZONTAL DISPLACEMENT (mm)	VERTICAL DISPLACEMENT (mm)
Gyroid	150	61	0.4	18	0.45	0.38
Gyroid	150	61	0.4	18	1.49	1.19
Gyroid	150	61	0.4	18	0.54	0.32
Gyroid	150	61	0.4	18	1.37	0.77
Gyroid	150	61	0.4	18	0.26	0.17
Gyroid	150	61	0.4	18	0.65	0.43
Gyroid	150	61	0.4	18	0.21	0.13
Gyroid	150	61	0.4	18	0.35	0.23
Gyroid	150	61	0.4	18	0.24	0.16
Gyroid	150	61	0.4	18	0.12	0.09
Gyroid	150	61	0.4	18	0.06	0.03
Schwarz	150	61	0.4	18	0.18	0.09
Schwarz	150	61	0.4	18	0.26	0.14
Schwarz	150	61	0.4	18	0.27	0.15
Schwarz	150	61	0.4	18	0.73	0.42
Schwarz	150	61	0.4	18	0.15	0.18
Schwarz	150	61	0.4	18	0.35	0.46
Schwarz	150	61	0.4	18	0.11	0.06
Schwarz	150	61	0.4	18	0.14	0.08
Schwarz	150	61	0.4	18	0.23	0.14
Schwarz	150	61	0.4	18	0.43	0.28
Schwarz	150	61	0.4	18	0.11	0.09
Schwarz	150	61	0.4	18	0.26	0.21
Schwarz	150	61	0.4	18	0.07	0.05
Schwarz	150	61	0.4	18	0.08	0.07
Schwarz	150	61	0.4	18	0.15	0.14
Schwarz	150	61	0.4	18	0.04	0.02

UNIT CELL TYPE	HORIZONTAL DISPLACEMENT / VERTICAL DISPLACEMENT	HORIZONTAL DISPLACEMENT * DENSITY	VERTICAL DISPLACEMENT * DENSITY	VERTICAL DEFORMATION	HORIZONTAL DEFORMATION	VERTICAL STIFFNESS [MPa]	HORIZONTAL STIFFNESS [Mpa]	VON MISES STRESS (Pa)	VON MISES STRESS * DENSITY
Gyroid	1.18	0.15	0.13	3%	1%	5.53	3.66	2.24E+06	7.39E+05
Gyroid	1.25	0.19	0.16	9%	4%	1.76	1.11	6.97E+06	9.11E+05
Gyroid	1.69	0.15	0.09	3%	2%	5.63	3.53	3.12E+06	8.89E+05
Gyroid	1.78	0.19	0.11	6%	4%	2.34	1.39	7.02E+06	9.94E+05
Gyroid	1.53	0.10	0.06	2%	1%	8.82	7.11	3.20E+06	1.18E+06
Gyroid	1.51	0.12	0.08	4%	2%	3.49	2.84	5.09E+06	9.26E+05
Gyroid	1.62	0.07	0.04	2%	1%	9.23	9.08	2.27E+06	7.31E+05
Gyroid	1.52	0.07	0.05	3%	1%	5.22	5.45	3.60E+06	7.68E+05
Gyroid	1.50	0.06	0.04	2%	1%	6.56	7.94	3.48E+06	8.50E+05
Gyroid	1.33	0.04	0.03	2%	0%	10.00	15.40	1.62E+06	4.97E+05
Gyroid	2.00	0.02	0.01	1%	0%	16.00	32.80	1.92E+06	5.48E+05
Schwarz	2.00	0.11	0.06	1%	1%	20.00	10.59	2.02E+06	1.25E+06
Schwarz	1.86	0.13	0.07	1%	1%	12.86	7.33	6.25E+06	3.04E+06
Schwarz	1.80	0.12	0.07	1%	1%	13.00	7.06	1.72E+07	7.73E+06
Schwarz	1.74	0.18	0.11	4%	2%	4.29	2.61	4.13E+06	1.04E+06
Schwarz	0.83	0.09	0.10	2%	0%	8.33	12.32	1.64E+06	9.47E+05
Schwarz	0.76	0.11	0.15	5%	1%	3.26	5.28	2.34E+06	7.54E+05
Schwarz	1.83	0.06	0.03	1%	0%	20.00	17.33	967980	4.89E+05
Schwarz	1.75	0.06	0.04	1%	0%	15.00	13.62	1.38E+06	6.04E+05
Schwarz	1.64	0.07	0.04	2%	1%	8.57	8.29	2.61E+06	7.87E+05
Schwarz	1.54	0.08	0.05	4%	1%	4.29	4.43	3.50E+06	6.58E+05
Schwarz	1.22	0.05	0.04	1%	0%	11.67	17.33	1.97E+06	8.21E+05
Schwarz	1.24	0.06	0.05	3%	1%	5.00	7.33	1.60E+07	3.44E+06
Schwarz	1.40	0.03	0.02	1%	0%	18.00	26.41	1.66E+06	7.95E+05
Schwarz	1.14	0.03	0.03	1%	0%	12.86	23.11	2.10E+06	8.76E+05
Schwarz	1.07	0.04	0.04	2%	0%	6.43	12.32	3.13E+06	8.42E+05
Schwarz	2.00	0.01	0.01	1%	0%	24.00	46.21	3.24E+06	1.11E+06

TPU Filament Datasheet:

1

FDM TPU 92A

FDM® TPU 92A is a thermoplastic polyurethane with a Shore A value of 92. The material exhibits high elongation, superior toughness, durability and abrasion resistance.

FDM TPU 92A brings the benefits of elastomers to FDM 3D printing and offers the capability to quickly produce large and complex elastomer parts. Typical applications include flexible hoses, tubes, air ducts, seals, protective covers and vibration dampeners.

FDM TPU 92A is available on the F123™ Series 3D Printers and is compatible with QSR™ soluble support material.

Mechanical Properties	Test Method	Value	
		XY Orientation	XZ Orientation
Shore Hardness (molded)	ASTM D2240	92 Shore A	92 Shore A
Tensile Strength, Yield (Type 1, 0.125", 0.2"/min)	ASTM D412	15.6 MPa (2,265 psi)	16.1 MPa (2,332 psi)
Tensile Strength, Ultimate (Type 1, 0.125", 0.2"/min)	ASTM D412	16.8 MPa (2,432 psi)	17.4 MPa (2,519 psi)
Tensile Modulus (Type 1, 0.125", 0.2"/min)	ASTM D412	15.3 MPa (2,212 psi)	20.7 MPa (3,000 psi)
Elongation at Break (Type 1, 0.125", 0.2"/min)	ASTM D412	552%	482%
Elongation at Yield (Type 1, 0.125", 0.2"/min)	ASTM D412	466%	385%
Tensile Stress at 100% Elongation (PSI)	ASTM D412	6.9 MPa (999 psi)	7.6 MPa (1,096 psi)
Tensile Stress at 300% Elongation (PSI)	ASTM D412	11.0 MPa (1,598 psi)	11.9 MPa (1,722 psi)
Flexural Strength (Method 1, 0.05"/min)	ASTM D790	1.8 MPa (255 psi)	2.4 MPa (351 psi)
Flexural Modulus (Method 1, 0.05"/min)	ASTM D790	25.6 MPa (3,719 psi)	36.9 MPa (5,349 psi)
Flexural Strain at Break (Method 1, 0.05"/min)	ASTM D790	No break	No break
Tear Strength - Stamped	ASTM D624-C	84.6 N/mm (483 lbF/in)	NA
Compressive Strength, Yield (Method 1, 0.05"/min)	ASTM D695	2.6 MPa (384 psi)	2.6 MPa (384 psi)
Compressive Strength, Ultimate (Method 1, 0.05"/min)	ASTM D695	2.6 MPa (384 psi)	2.6 MPa (384 psi)
Compressive Modulus (Method 1, 0.05"/min)	ASTM D695	16.9 MPa (2,457 psi)	16.9 MPa (2,457 psi)
Compression Set at 22 Hours @ 23 °C	ASTM D395	21%	NA
Compression Set at 22 Hours @ 70 °C	ASTM D395	44%	NA

Data Sheet

FDM TPU 92A

Thermal Properties	Test Method	Value
Heat Deflection (HDT) @ 66 psi	ASTM D648	38 °C (100.4 °F)
Heat Deflection (HDT) @ 15 psi	NA	56 °C (132.8 °F)
Vicat Softening Temperature (Rate B/50)	ASTM D1525	95 °C (203 °F)
Glass Transition Temperature (Tg)	DMA (SSYS)	-42 °C (-43.6 °F)
Coefficient of Thermal Expansion (x-direction)	ASTM E831	139 µm/(m·°C) (7.72E-05 in/(in·°F))
Coefficient of Thermal Expansion (y-direction)	ASTM E831	159 µm/(m·°C) (8.83E-05 in/(in·°F))
Coefficient of Thermal Expansion (z-direction)	ASTM E831	176 µm/(m·°C) (9.78E-05 in/(in·°F))

Electrical Properties	Test Method	Value	
		XY Orientation	XZ Orientation
Volume Resistivity	ASTM D257	6.09E+10 ohm-cm	7.17E+13 ohm-cm

Other	Test Method	Value
Specific Gravity	ASTM D792	1.13502

Stratasys Headquarters

7665 Commerce Way,
Eden Prairie, MN 55344
+1 800 801 6491 (US Toll Free)
+1 952 937-3000 (Intl)
+1 952 937-0070 (Fax)

stratasys.com
ISO 9001:2008 Certified

1 Holtzman St., Science Park,
PO Box 2496
Rehovot 76124, Israel
+972 74 745 4000
+972 74 745 5000 (Fax)